Tungsten Carbide-Cobalt by Three Dimensional Printing

by

ANDREW KELLEY, III

B.S. Mechanical Engineering
North Carolina State University, 1996

Submitted to the Department of Mechanical Engineering
in Partial Fulfillment of the
Requirements for the Degree of

MASTER OF SCIENCE IN MECHANICAL ENGINEERING

at the

Massachusetts Institute of Technology

June 1998

Signature of Author _____
Department of Mechanical Engineering
May 8, 1998

Certified by _____
Emanuel M. Sachs
Professor of Mechanical Engineering
Thesis Supervisor

Accepted by _____
Ain A. Sonin
Chairman, Graduate Committee

Tungsten Carbide-Cobalt by Three Dimensional Printing

by

Andrew Kelley, III

Submitted to the Department of Mechanical Engineering
on May 8, 1998 in Partial Fulfillment of the
Requirements for the Degree of Master of Science in
Mechanical Engineering

ABSTRACT

Three Dimensional Printing is an additive manufacturing process for rapid prototyping ceramic and metallic parts [Sachs, et al, 1990]. Green (not sintered) tungsten carbide-cobalt parts must have a density greater than 50% of the theoretical density, 14.9 g/cc, for proper sintering and post-processing. Two approaches were assessed for feasibility and robustness: printing slurry into tungsten carbide-cobalt spray dried powder and printing a solvent in spray dried tungsten carbide powder that readily dissolves.

For slurry administered to a powder bed of solid, spherical particles, it has been found that the resulting packing primitive packing fraction increases almost linearly with the volume loading of the slurry over a range of powder size. The increase in density is approximately half what would be calculated by assuming that the slurry fills all the porosity in the powder bed. The maximum green density achieved by printing slurry into a spray dried tungsten carbide-cobalt bed was 41%, midway between the lower bound calculated by assuming the vehicle in the slurry infiltrates only the large pores between the spray dried power and the upper bound calculated by assuming that the vehicle of the slurry also infiltrates the find pores within a spray dried granule.

A re-dispersible spray dried powder (38-53 micron size range) was fabricated using only the Duramax 3007 dispersant as the binder. This powder redisperses in water. Administering a drop of water to this powder resulted in primitives with 47% packing density, but which had significant quantities of 80 micron voids. Several lines of evidence pointed to the hypothesis that the voids were the result of trapped air. Two methods were successfully employed to nearly eliminate such voids. In one approach, the droplet of water was administered to the powder bed under a vacuum of between 25 and 40 torr and air was admitted to the chamber to 1 atmosphere after different intervals of time ranging from 30 seconds to 10 minutes.

In another approach, the ability of water to absorb CO_2 was used to "getter" any trapped gas into the liquid. Water was administered to a powder bed under a CO_2 environment at room temperature. After a 2 minute period, intended to allow the spray dried powder to substantially re-disperse, the temperature of the powder bed was lowered to 0-5 degrees Centigrade in order to increase the amount of CO_2 which could be absorbed in the water and "switch on" the gettering of the trapped gas. Controls were run with the same procedure in air. The primitives made under CO_2 were nearly void free and had green densities as high as 52%, while the controls were not significantly different than primitives made at room temperature in air.

Thesis Supervisor: Dr. Emanuel M. Sachs
Title: Professor of Mechanical Engineering

ACKNOWLEDGMENTS

I would like to acknowledge the support of the National Science Foundation.

Ely Sachs thank you for catalyzing my determination and teaching me to recast complexity in the eloquence of simplicity.

John Keane, John Friederichs thanks for your vote of confidence and continuing support.

Jim Serdy, Dave Brancazio, Luara Zaganjori thanks for all of the support, the laughs and the expert advice.

Jason Grau, Jooho Moon, Lenny Rigione, the residents of building 12 thanks for your patience in introducing me to ceramics and vital resources.

Adam Lorenz, Akan Oton, Akobouije Chijouke, Vedran Knezevic, Stefan Koch, Xiaorong Xu, Honglin Guo, thanks for your friendship, advice and inspiration. It was a pleasure working with such a talented group of intellectually stimulating peers.

Fred Cote thanks for your friendship and indefatigable dispensation of timely manufacturing knowledge.

TABLE OF CONTENTS

LIST OF FIGURES

LIST OF TABLES

1.0 INTRODUCTION

1.1 THREE DIMENSIONAL PRINTING

Three Dimensional Printing is an additive manufacturing process for rapid prototyping ceramic and metallic parts [Sachs et al, 1990]. Material in powder form that can be easily spread may serve as a bed for 3D Printing (3DP). The current build volume is 6" x 12" x 12". Figure 1 shows a pair of rocker arms being made by the 3DP process [Baker]. Parts are produced by spreading 170 micron layers of powder and selectively binding regions of the powder bed.

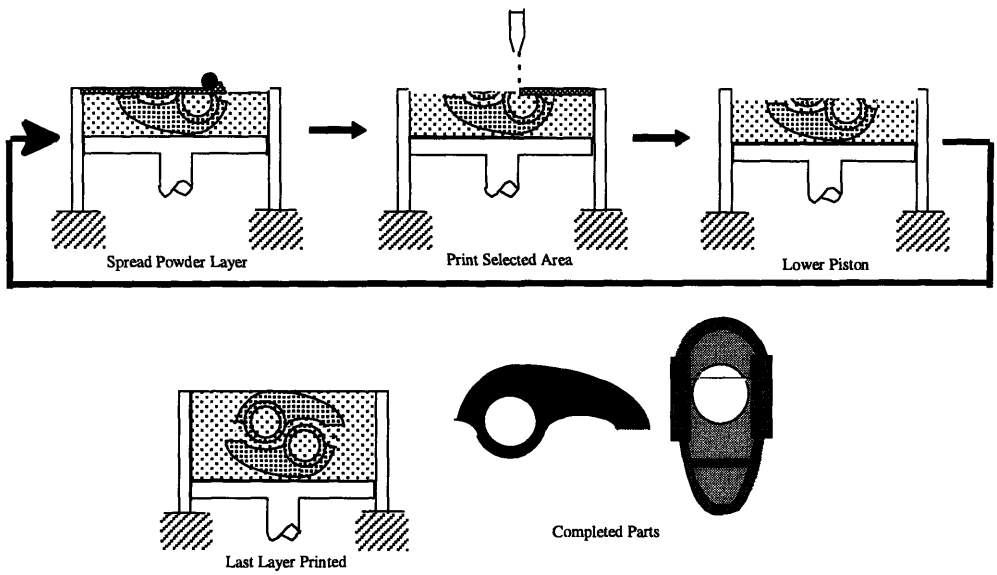

Figure 1.1 - The 3DP Process

1.2 MOTIVATION AND GOALS

Tungsten carbide-cobalt has a variety of important industrial applications. Many ceramic products may be enhanced by applying the 3DP process to the tungsten carbide-cobalt material system. Also, cycle time from new product design to test may be shortened and tooling dies and punches may be fabricated more quickly [Keane, 1997].

Industrial focus areas include:

I. *Die and wear parts*, especially those with complex features or internal cooling channels

II. *Cutting tool inserts* whose attributes include:

   A. Complex features which are difficult or expensive to grind

   B. Precision parts (no grind)

   C. Functionally gradient materials

   D. Regional material reinforcement

The goal of this work was to produce un-sintered green parts with a packing fraction in excess of 0.50. Such packing fractions preclude the costly requirement of isostatic pressing before sintering.

1.3 APPROACH AND METHODS

Two approaches were assessed:

1. administering slurry to a powder bed, and,
2. administering liquid to highly designed spray dried powder with a high propensity to re-disperse.

The flow chart in Figure 1.1 graphically outlines the work presented. The rightmost vein was selected as the most promising after the completion of a preliminary assessment of both veins.

Slurries were formulated by combining variegated WC dispersants with different liquid vehicles. Well-dispersed slurries up to 60 volume percent were made. Powders used included WC, spray dried WC and WC/Co, Spheriglas beads and cellulose. Highly designed spray dried powder was produced since commercially available spray dried powders are not suitable for direct 3DP application.

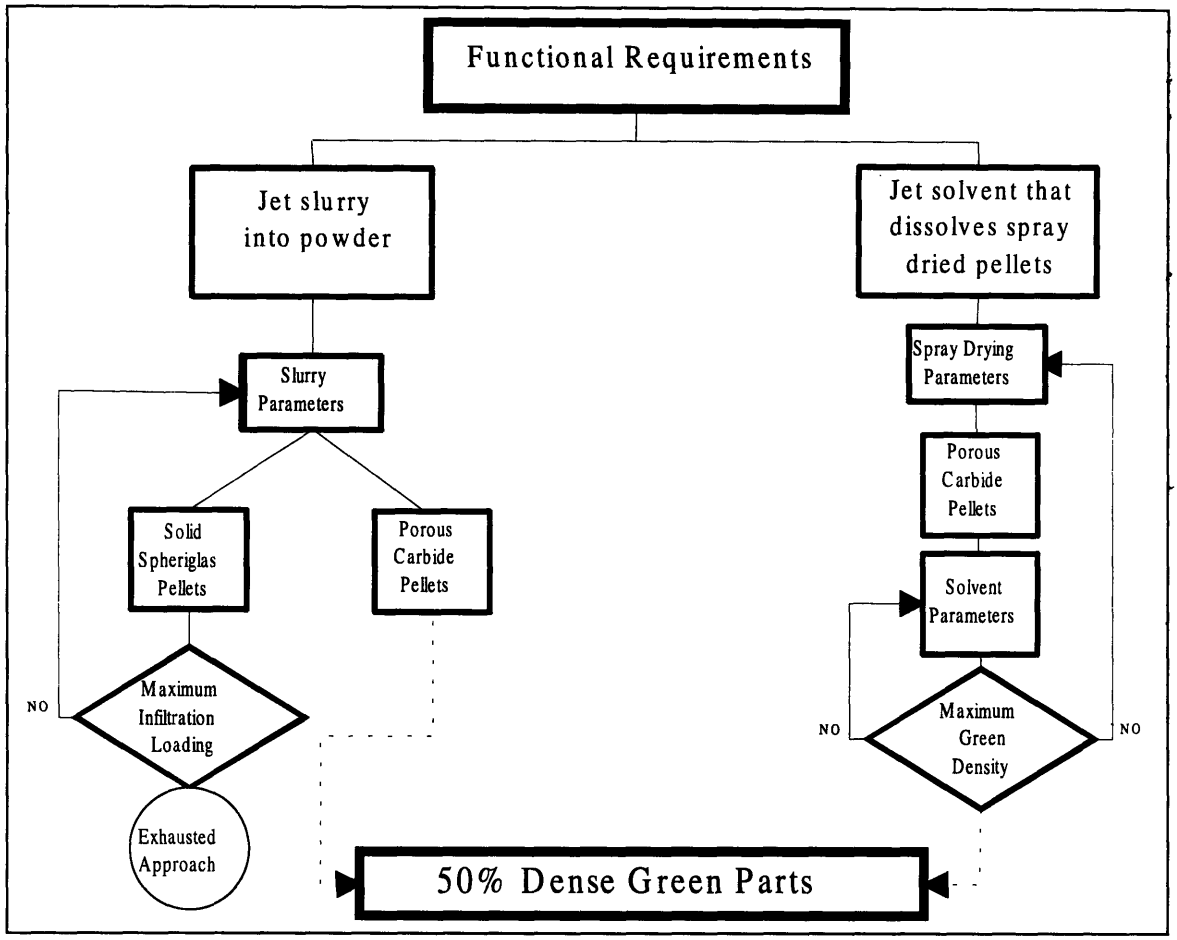

Figure 1.2 -- WC/Co Project Paths

1.4 ORGANIZATION

The layout of this thesis is synopsized as follows. Chapter 2 discusses spray dried powder. Chapter 3 briefly describes WC slurry. Chapter 4 details the interaction between slurry infiltrant and powder composed of solid pellets. Chapter 5 highlights highly designed spray dried powder made within 3DP. Chapter 6 presents conclusions and suggestions for further research. Appendix A discusses the infiltration dynamics of porous pellets. Appendix B describes slurry infiltration of 100 micron cellulose powder. Appendix C highlights an infiltration search based on the premise that reduced infiltration time defeats balling. Appendix D chronicles ink jet spray drying.

2.0 SPRAY DRIED POWDER

2.1 SPRAY DRYING

Tungsten carbide-cobalt (WC/Co) is available as raw powder and spray dried powder. Raw powder typically ranges from 0.8 to 15 microns in size. Enhanced green part sintering and final part fracture toughness necessitate small particles with large surface area–to-volume ratios. The raw powder often contains large agglomerates unsuitable for spreading in the 3DP Alpha machine. For this reason spray dried powder must be used.

Spray drying accomplishes the required conversion from slip [slurry] to powder in a single, continuous, automatically controlled step. In addition, powder properties can be controlled in terms of particle size, flowability, apparent density, and moisture content [Shaw]. More information on spray drying WC using a Niro atomizer unit is given in Chapter 5.

2.2 TUNGSTEN CARBIDE-COBALT SPRAY DRIED POWDER

After tungsten (W) is carburized, its fracture toughness is improved by adding 6 to 17 percent cobalt. Typically, spray dried powder pellets are held together by a few d.w.p. of an organic binder such as polyethylene glycol or acrylic [Benjamin]. Depending upon the binder and particle size, tungsten carbide-cobalt spray dried powder can be highly flow-able.

The spray dried WC/Co powders manufactured by Osram Sylvania and a different manufacturer had mean diameters of 100 and 200 microns, respectively. Steel meshes were used to manually classify the powder with the distribution shown in Table 2.1.

Mesh Opening (microns)	Percentage Below for PEG WC/Co Spray Dried Powder (Osram Sylvania)	Percentage Below for Hydrophobic WC/Co Spray Dried Powder
180	31	58
250	91	99
500	100	100

Table 2.1 -- Spray Dried Powder Size Classification

The PEG spray dried WC/Co was hollow. In addition, it did not tend to rearrange to any significant degree. Figure 2.1 shows PEG spray dried powder supplied by Osram Sylvania after it had been saturated with water and dried. Although some disintegration of the pellets was evident, gross rearrangement was not. The packing fraction of the resulting cake, 0.29, was only marginally higher than the apparent density of the loose bed, 0.26. In sum, these pellets do not redisperse to any appreciable degree.

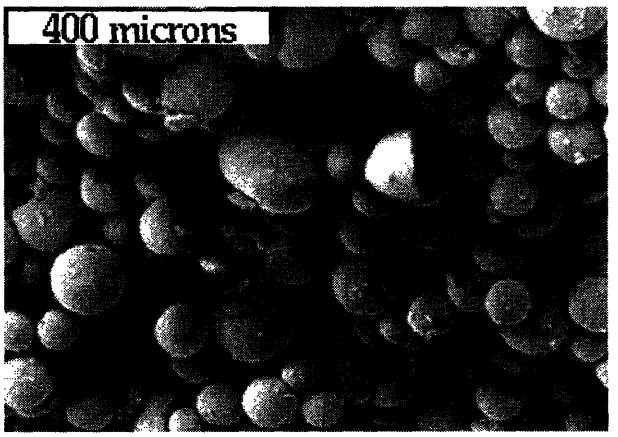

Figure 2.1 -- Water Saturated and Dried PEG Spray Dried WC/Co

2.3 ANGLE OF REPOSE

In the 3DP process, before layers can be printed, powder must be spread. Even spreading places limitations on the flow-ability of usable powder. One of the key measures of flow-ability of spray dried powder is the angle of repose. See Table 2.2. Angle of repose varies inversely with flow-ability.

Spray Dried Powder	Binder	Angle of Repose
WC	None	27°
WC/Co	Polyethylene glycol (PEG)	27°
WC/Co	Hydrophobic Binder	34°

Table 2.2 -- Angle of Repose for Different Spray Dried Powders

2.4 APPARENT AND TAP DENSITY

The following is a short list of standard definitions as adapted from the ASM Handbook, Volume 7, Powder Metallurgy. All are typically expressed in units of grams per cubic centimeter.

apparent density	--	weight of a unit volume of powder
bulk density	--	same as apparent density
green density	--	density of an unsintered part composed of bound powder
tap density	--	weight of a unit volume of powder after vibrating

Apparent density is a lower bound on the non-compacted powder bed density. Apparent density was measured by adding a known mass of powder to a dry, demarcated graduated cylinder. Tap density is a measure of the density of compacted powder and is usually higher than the apparent density of the same powder. The method for measuring tap density simulated ASTM B 527 standards. For comparison, sub-micron powder is also shown in Table 2.3. Tap density data was not collected for any of the Niro spray dried powder since that powder was in short supply.

Powder	Binder	Apparent Density (g/cc)	Tap Density (g/cc)
Sub-micron WC	None	3.3	4.9
Spray Dried WC/Co	Hydrophobic Binder	3.2	3.7
Spray Dried WC/Co	PEG	3.8	4.3
38-53μm Spray Dried WC[1]	None	3.8	---
53-88μm Spray Dried WC[2]	None	4.2	----

Table 2.3 -- Apparent and Tap Density of Tungsten Carbide Powders

[1]Powder obtained from first Niro spray drying run. [2]Second run powder.

2.5 PACKING FRACTION AND POROSITY

For a powder bed, packing fraction is the apparent density of the bed divided by the true density of the bed constituents. Consider solid Spheriglas beads with a true density of 2.5 g/cc. Since these beads pack to approximately 60 % within the bed, the green density is 1.5 g/cc. Now, consider a spray dried pellet with 50% porosity. If pellets such as this pack to 50 v/o in the bed, then the overall packing fraction of the bed is 25%. Therefore, the bed porosity would be 75%. In summation,

$$f_{packing} = \frac{ApparentDensity}{TrueDensityofBedConstituents}$$

$$porosity = 1 - f_{packing}$$

The true density of 0.8 micron WC is 14.9 g/cc. The powder also contains trace elements of vanadium carbide and titanium carbide to enhance sintering. Table 2.4 shows the packing fraction calculated by dividing the powder apparent density by the true density.

Powder	Binder	Packing Fraction
Sub-micron WC	None	0.22
Spray Dried WC/Co	Hydrophobic binder	0.21
Spray Dried WC/Co	PEG	0.26
38-53μm Spray Dried WC[1]	None	0.26
53-88μm Spray Dried WC[2]	None	0.28

Table 2.4 -- Packing Fraction for Various WC and WC/Co Powders

[1]Powder obtained from first Niro spray drying run. [2]Second run powder.

2.6 MERCURY POROSIMETRY

Spray dried particles are agglomerations of smaller particles, therefore, individual pellets are not fully dense. Furthermore, pellets may be dimpled, hollow or even crescent-shaped. Knowing the degree of uniformity throughout a representative spray dried pellet facilitates optimization of spray drying process parameters. Mercury (Hg) porosimetry is suited for measuring the density of individual spray dried pellets and primitives smaller than can be practically weighed and measured [Bredt, Ph.D. Thesis]. Mercury

porosimetry was developed from the need to measure the pore size distribution in porous construction materials with a wide range of pore sizes [Ashurst & Klar].

An Autopore 9220 manufactured by Micromeritics Corporation in Hialeah, Florida was used to perform mercury porosimetry. Essentially, porosimetry allows for the determination of a 'shrink-wrapped' volume of a known sample mass. This volume corresponds to the volume to be used in the calculation of the apparent density of the sample. Figure 2.2 shows mercury porosimetry data for the spray dried WC. This powder was produced during the first Niro spray drying run and was classified so as to be 38-53 microns. The plot given is typical for spray dried WC powder.

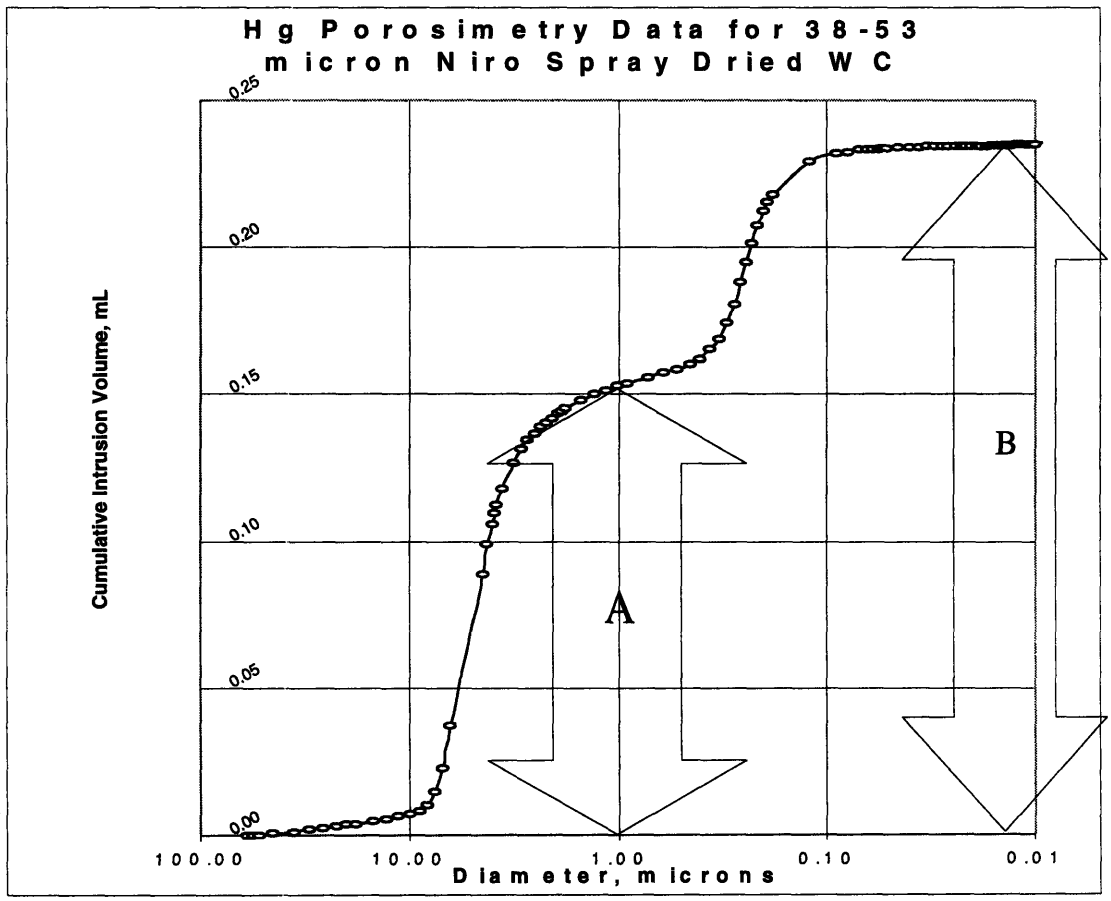

Figure 2.2 -- Porosimetry Data for the 38-53 micron Niro Spray Dried WC

As mercury infiltrates the sample the cumulative intrusion volume increases. The diameter on the abscissa is calculated from the pressure required to force the mercury into the sample. For soft samples like friable spray dried powder, this plateau will tail upward as the porosimetry pressure, which ranges up to 60 ksi, crushes the sample.

The first plateau, at elevation A, corresponds to the point at which the preponderance of, at elevation B, corresponds to the point at which no more mercury can fill the sample. The ratio of these plateaus gives and indication of how many large pores exist in the sample relative to small pores. The large pore fraction is defined as A divided by B. Let,

A = total volume of large pores in the sample, and,

B = total volume of all pores in the sample.

Then

$$\text{Large Pore Fraction} = \frac{A}{B}$$

And in this particular case,

$$\text{Large Pore Fraction} = \frac{0.15}{0.24}$$

$$\text{Large Pore Fraction} = 0.63.$$

Note that the value of B will be underestimated by mercury porosimetry if enclosed porosity exists.

Porosimetry also provides a qualitative characterization of the sample pore structure, which is often informative in subsequent analyses of parts. Pore size distribution data generated by mercury porosimetry are primarily useful in comparative studies of similar materials. Mercury porosimetry has proved to be an effective tool for separating interparticle voids and internal particle porosity. However, note that mercury porosimetry does tends to underestimate the sample pore size. This is due to constrictive

pores and "ink bottle" filling [Ibid.]. The filling of 100 micron spheres after mercury infiltrates a sub-micron capillary is an extreme example of ink-bottle filling.

The steepest slopes in Figure 2.2 indicate two major characteristics of the powder:

1) interparticle voids -- the pores between the spray dried particles, and,
2) internal particle porosity -- the pores within the spray dried particles.

The interparticle pores of the powder range from 3 to 8 microns. Generally, this range will increase with the size of the spray dried powder sampled. These pores are usually one order of magnitude less than the spray dried powder sample size.

The internal particle pores are submicron as expected. These pores range from 0.2 to 0.4 microns. This range will remain roughly the same for different sizes of spray dried WC if the slip solids consist of submicron WC. Large internal voids may coexist with these small interparticle pores. Figure 2.3 shows a cross section of the PEG spray dried WC/Co supplied by Osram Sylvania. The section was made by fixing the spray dried powder in epoxy. The epoxy-powder sample was then ground.

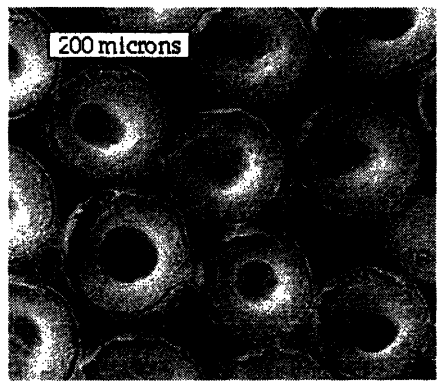

Figure 2.3 -- Internal Voids in Osram Sylvania PEG Spray Dried WC/Co

Additional information on porosimetry calculations is presented in Appendix E.

3.0 TUNGSTEN CARBIDE SLURRY

3.1 SUBMICRON WC POWDER

Submicron tungsten carbide powder was supplied for this project. This powder was used in the preparation of all of the WC slurries mentioned in this work. Figure 3.1 shows a detail of the submicron powder as seen in an aqueous 25 v/o WC, 1.8 d.w.p. Duramax 3007 slurry that was slip cast onto a plaster block. The powder particles were approximately 0.8 microns equiaxed platelets. Note that the highest packing fractions result from spherical particles.

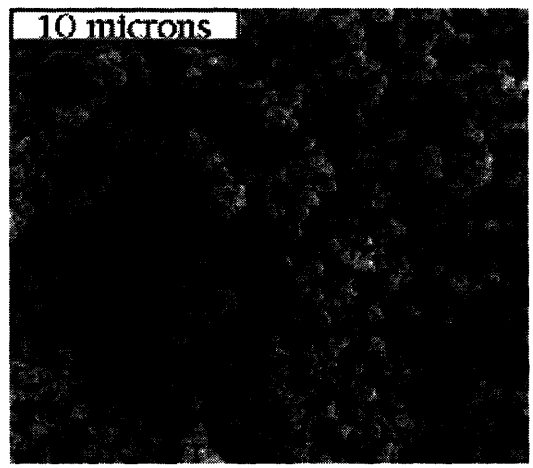

Figure 3.1 -- Top Surface of a Slip Casting Showing 0.8 microns Tungsten Carbide Particles

3.2 VEHICLE AND DISPERSANT SELECTION

Several vehicle/dispersant systems have been used to make slurries of WC during the course of the WC/Co project. Vehicles have included heptane, Multitherm 503, and water. Oloa 1200, Darvan-C and Duramax are some of the dispersants that have been used.

For experimentation involving jetting slurry into hydrophobic binder spray dried WC/Co, the Multitherm/Oloa system was used. This system actually exhibited better infiltration, as indicated by the maximum infiltration loading, than a highly loaded aqueous system. While 52 v/o aqueous WC could be made to infiltrate 119 micron Spheriglas beads, 60 v/o WC could be made to infiltrate the same beads using the Multitherm/Oloa system. In

both cases, even higher solids concentrations could be obtained, however, these could not be made to infiltrate the powder.

Figure 3.2 shows a fractograph of a primitive that was made by infiltrating 119 micron Spheriglas with 60 v/o WC, 1.8 dry weight percent (d.w.p.) Oloa 1200 in Multitherm 503. The primitive was made by administering the slurry through a 330 micron nozzle affixed to a syringe.

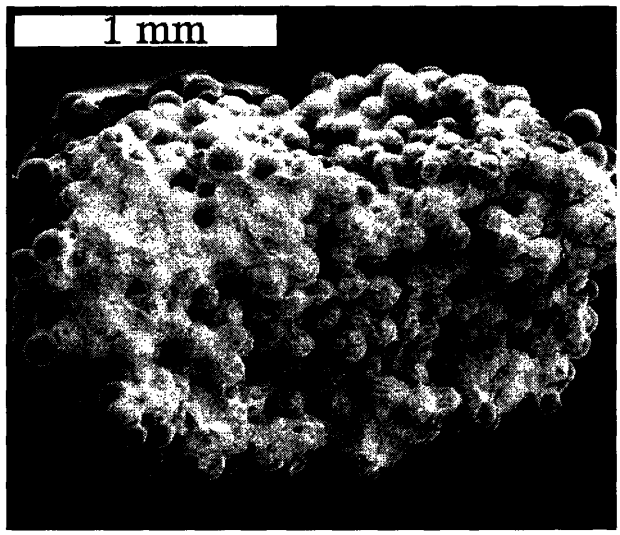

Figure 3.2 -- 60 v/o WC, 1.8 d.w.p. Oloa, Multitherm into 119 micron Spheriglas Fractograph

After sintering, some of the Oloa in the system might remain and this was one of the gating issues in the development of a Multitherm/Oloa system. In addition, non-aqueous based solvents are not preferred on the 3DP Alpha machine. For this reason, work was done to develop an aqueous based system. As a result, this required that spray dried powders of interest would have to be hydrophilic. Note that polyethylene glycol is hydrophilic which means aqueous slurries may be used for infiltration.

Aqueous Duramax 3007 slurry exhibited excellent handling and jetting properties. Good aqueous dispersions have been made using 1.8 d.w.p. Duramax 3007 [Caradonna].
Figure 3.3 shows a fractograph of aqueous 52 v/o WC, 1.8 d.w.p. Duramax 3007 after infiltration into 119 micron Spheriglas beads.

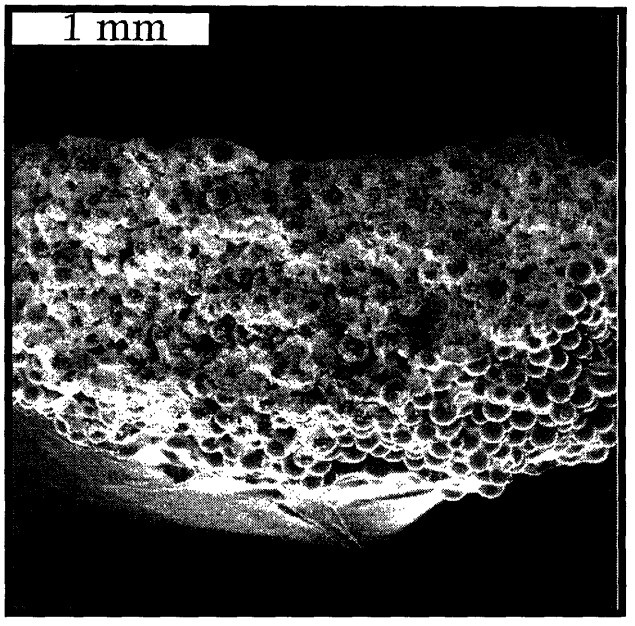

Figure 3.3 -- Aqueous 52 v/o WC, 1.8 d.w.p. Duramax 3007 into 119 micron Spheriglas Fractograph

3.3 SLURRY PREPARATION AND SETTLING TIME

For aqueous slurries with 1.8 d.w.p. Duramax, the best dispersions are produced if a mechanical stirrer is used during preparation. This method will produced markedly improved results as compared to using a magnetic stir bar for solids concentrations above 20 volume percent. Thereafter, a minimum ball milling time of approximately six hours is required for slurry stability. For more information on the preparation of highly loaded slurries refer to Koch.

4.0 SOLID POWDER INFILTRATION

This chapter lays the foundation of the first approach to making WC/Co parts by 3DP. The goal was to jet slurry into a bed of powder. WC slurry will infiltrate the powder bed void space if the solids loading is low enough. Capillary pressure, which easily reaches several atmospheres in the powder bed drives infiltration. Figure 4.1 shows a drop of slurry infiltrating solid beads. Single drop primitive features were made by administering slurry with a syringe through either a 152 or 330 micron nozzle as noted.

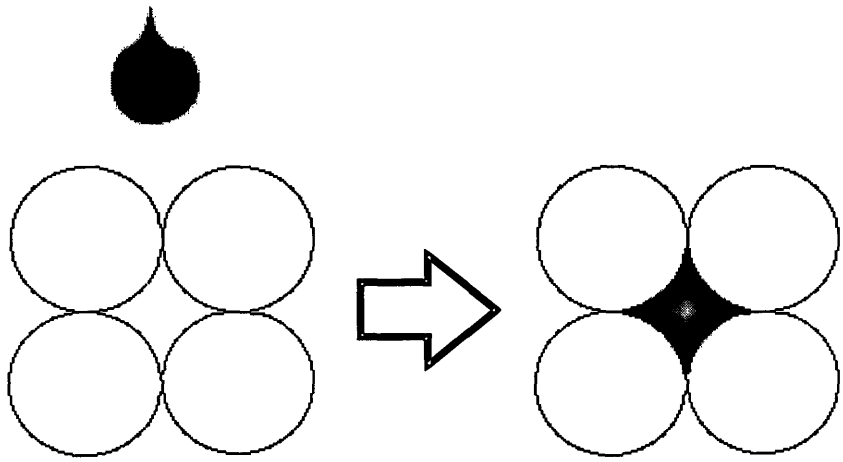

Figure 4.1 - Slurry Infiltrating Beads

4.1 DRIED INFILTRANT UPPER BOUND

The upper bound on the dried infiltrant packing fraction is the packing fraction of the corresponding slip casting. See Table 4.1. This bound, 52%, was taken to be the new goal of the project, which had previously been set at 55%.

Solids Loading (%)	Slip Casting Packing Fraction (---)
10	0.52
25	0.48
52	0.52

Table 4.1 - Slip Cast Aqueous WC, 1.8 d.w.p. Duramax 3007 Slurry onto Plaster

Each slip casting was approximately one-eighth inch thick and one inch in diameter.

4.2 POST INFILTRATION DENSITY

For powder beds composed of solid beads calculating the density after infiltration is straightforward. Let

f	=	final packing fraction,
f_b	=	packing fraction of the solid beads in the bed, and,
s	=	volume fraction of slurry.

Then

$$f = f_b + s(1-f_b).$$

For example, for 25 v/o slurry administered to 85 micron Spheriglas beads:

$$f = 0.57 + (0.25)(1-0.57)$$

$$f = 0.68.$$

This value is higher than the measured value, 0.61, likely due to incomplete bed saturation.

This calculation above is not so simple for porous spray dried beads. First of all, liquid migrates faster in porous beads than in solid beads. Therefore, there is less time for slurry solids to settle into the bed. The second issue is whether or not liquid infiltrates the bead interior and, if so, on what time scale relative to the infiltration of the powder bed. For these reasons experiments were designed for slurry infiltration of *solid* beads first.

4.3 SPHERIGLAS BEAD SELECTION

A-Glass Spheriglas beads are solid soda-lime glass beads ranging in size from 7 to 203 microns. Spheriglas is readily available and manufactured by Potters Industries, Inc, P.O. Box 840, Valley Forge, PA 19842. Spheriglas beads have a true density of 2.5 g/cc as received.

Table 4.2 shows measured apparent densities for different Spheriglas sizes. Note that packing fraction increases with particle size.

Mean Bead Size (microns)	Apparent Density (g/cc)	Packing Fraction[1] (---)
42	1.39	0.56
85	1.42	0.57
119	1.46	0.58

Table 4.2 – Spheriglas Bead Properties

[1]The packing fraction corresponds to the apparent density.

Smaller flaws after printing increase the opportunity for success. John Friederichs allowed that internal flaws 120 to 200 microns should vanish during a tungsten-carbide cobalt sinter-hip process. When printing slurry into spherical beads, large flaws will result if slurry does not fill the space between the beads. The size of the space between the beads is directly related to the size of the beads. Therefore, decreasing the size of the beads will decrease the maximum internal flaw size. The minimum feature size of a 3DP part is limited to roughly twice the size of the powder; hence, the smallest powder that is flow-able should be used. Twenty micron beads were prone to caking do to atmospheric humidity and were not considered to be robust enough for future work. Forty-two micron Spheriglas does not cake at typical room temperature and humidity.

4.4 MAXIMUM INFILTRATION LOADING

The maximum slurry solids loading that could be made to infiltrate was determined for each of the Spheriglas sizes in Table 4.3. For example, for the 42 micron beads, 22 v/o slurry was heated and stirred to drive off excess water until the resulting slurry could no longer be made to infiltrate the powder. The slurry was then brought to room temperature. The slurry solids loading was inferred from the measured slurry density. The density was measured by weighing 3 cc of the slurry in a syringe. This approach allowed the maximum infiltration loading to be arrived at quickly and efficiently.

Mean Bead Size (microns)	Maximum Infiltration Loading (v/o)
20	10
42	31
85	50
119	52

Table 4.3 - Maximum Infiltration Loading for Different Sizes of Spheriglas

4.5 DESIGNED EXPERIMENT FOR SOLID BEADS

The maximum infiltration loadings were used to normalize experiments to be performed across a variety of parameters, *including packing fraction, slurry infiltration time and primitive geometry*. The three solids loading levels for each bead size were chosen by multiplying each maximum loading by 0.2, 0.5 and 0.8. Table 4.4 shows the 3-level full factorial design matrix.

Run	Mean Bead Size (microns)	Slurry Solids Loading (v/o)
1	42	6
2	42	15
3	42	25
4	85	10
5	85	25
6	85	40

Table 4.4 - Design Matrix for Spheriglas Beads and Aqueous WC slurry

4.6 PACKING FRACTION

Table 4.5 shows the quantitative results along with the apparent density of the powder alone. In the table, when both apparent densities are given, the packing fraction shown is for forty-two micron Spheriglas beads. Apparent density was measured using mercury porosimetry or similar methods. The packing fraction was greater than the 52% goal for every experiment. However, tungsten carbide particles much greater than 1 sinter poorly.

Slurry Solids Fraction (---)	42 micron Spheriglas apparent density (g/cc)	42 micron Spheriglas Packing Fraction (---)	85 micron Spheriglas apparent density (g/cc)	85 micron Spheriglas Packing Fraction (---)
0.00	1.39	0.56	1.42	0.56
0.06	1.80	0.58	------	----
0.10	-----	----	1.77	0.59
0.15	1.95	0.59	-----	----
0.25	2.23	0.61	2.24	0.62
0.40	-----	----	2.86	0.66

Table 4.5 – Dependence of Packing Fraction on WC Slurry Solids Fraction

[1]This data is taken from apparent density data for the dry powder. Strictly speaking, it is not the same as if the powder were saturated with water and allowed to dry.

Figure 4.2 graphically depicts the results of Table 4.5. These results indicated that:

1. packing fraction increases near-linearly with slurry density,
2. packing fraction is independent of solid particle size for the same solids loading, and,
3. slurry saturated only 50% of the bed porosity for solid beads.

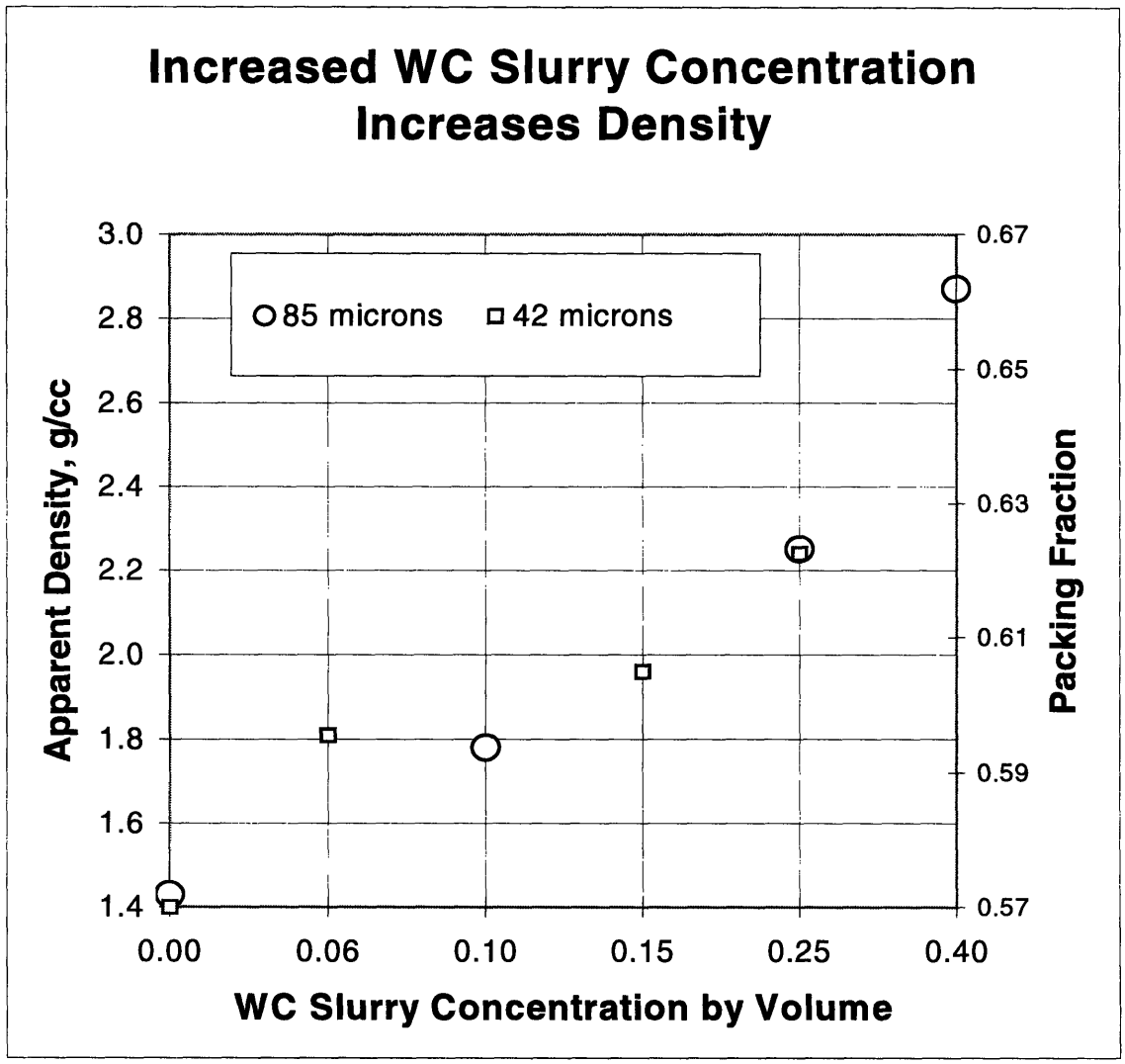

Figure 4.2 - Dependence of Packing Fraction on Slurry Solids Fraction

In each case, the density was measured using the alternative porosimetry method described in Appendix E.

The bed saturation for the 85 micron pellets was determined by comparing empirical results with theoretical predictions. A linear regression was performed for the WC-85 micron Spheriglas data. The regression included only the three data points for which slurry was administered to the bed. The empirical relation obtained was

$$\rho_{emp} = 1.38 + 3.63\, s_{WC}$$

where,

s_{WC} = tungsten carbide slurry solids fraction, and,
ρ_{emp} = empirically determined apparent density of a WC-85 micron Spheriglas primitive.

Let

ρ_{theo} = theoretical apparent density of a WC-85 micron Spheriglas primitive,
f = packing fraction of 85 micron Spheriglas,
ρ_{WC} = density of tungsten carbide slurry, and,
S = saturation of slurry in powder bed. This is the fraction of available pores which can be filled.

Then, theoretically, the density of a WC-85 microns Spheriglas primitive after the slurry dries is

$$\rho_{theo} = 1.42 + (1\text{-}f)\rho_{WC}\, s_{WC} S$$

Substituting values,

$$\rho_{theo} = 1.42 + (1\text{-}0.57)(14.9\ g/cc)s_{WC}S$$

By equating the theoretical and empirical apparent density equations, it was shown that

$$S = 0.56 - \frac{0.0062}{s_{WC}}$$

For solids fractions, s_{WC}, administered to the 85 micron beads the corresponding saturation ranged from 0.50 to 0.54. Similarly, for the 42 micron beads, saturation can be shown to be as low as 0.49. These values were much less than what was typical for single phase powder bed infiltration. Evidently, slurry particulates arrest the migration of liquid which would otherwise wet more of the bed in the absence of suspended particles.

4.7 INFILTRATION TIME, GEOMETRY AND INTERNAL FLAWS

Slurry infiltration time was less than 2 seconds in all cases. Primitives were less than 4 mm in diameter with a typical infiltration depth of 1 to 2 mm. Generally, for the same size powder, primitive size increased with decreased slurry concentration. This is because, as solids loading increases, the water in the slurry administered decreases. This smaller amount of water in the dosage, ceteris paribus, translated to less migration.

Scanning electron micrographs were taken of cross sections to qualitatively determine typical internal flaw size. Flaws were smallest in the experiments with higher solids loading. A more quantitative internal flaw size measurement method is needed. Enclosed porosity defeats the resolution and efficacy of all infiltration methods, such as mercury porosimetry.

4.8 MULTI-PASS PRINTING

It was theorized that multiple administrations of slurry might increase the powder bed. As the slurry liquid vehicle evaporates, void spaces remain that might be filled with more slurry. Therefore, the resulting packing fraction of a double-pass primitive should be higher than that for a single administrative. To assess the potential efficacy of this method, fractographs of primitives were inspected. Figure 4.3 shows 10 v/o WC slurry after infiltration into 42 micron Spheriglas beads. The open porosity at the top of the fractograph cross-section seemed to suggest that a second administration of slurry could be made to infiltrate.

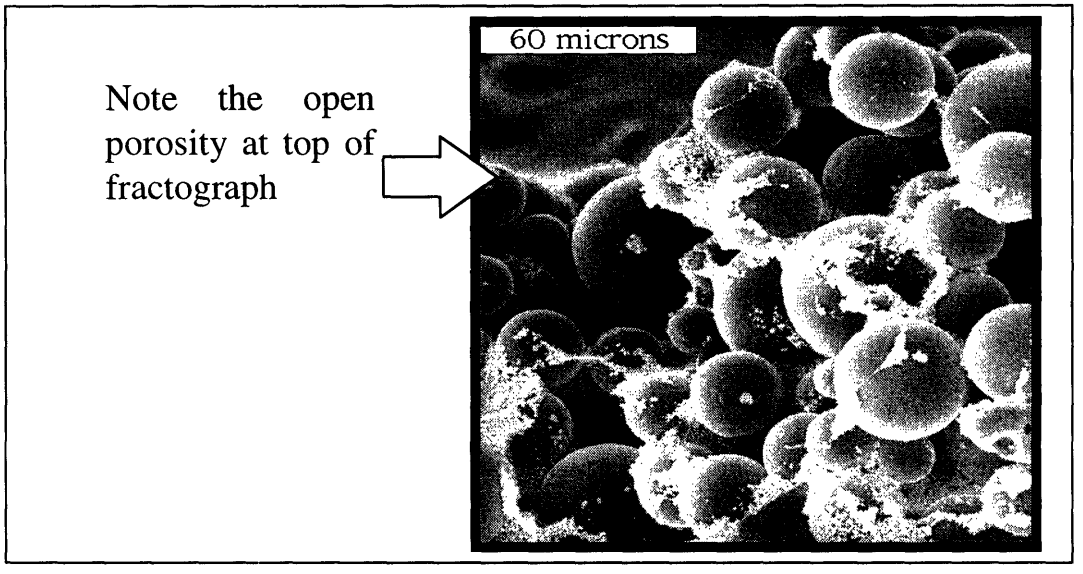

Figure 4.3 -- Aqueous 10 v/o WC, 1.8 d.w.p. Duramax into 42 micron Spheriglas

After a first administration of WC slurry was made to 85 micron Spheriglas beads, subsequent slurry could not be made to infiltrate the previously infiltrated region. Instead, the slurry bled into the surrounding region of the powder bed. Two methods were used to circumvent this problem:

1. extract the primitives from the bed and reprint, or,
2. print a sheet on the bed and reprint.

In the first approach, slurry tended to cast around the bead instead of infiltrating the section of the primitive where slurry was previously first introduced. In the second approach, the slurry tended to cast on the sheet without infiltrating. This approach was not successful for 40 v/o slurry double printed into 85 micron Spheriglas. For this approach to succeed, the final primitive packing fraction required could not have been obtained at lower solids loadings, theoretically. Exploration down this path was stopped in order to give more attention to more promising aspects of the WC/Co project.

5.0 DISSOLVING NIRO SPRAY DRIED PELLETS

This chapter outlines the second approach to producing high green density WC/Co parts. The method required administering a solution to a powder bed of pellets with a high propensity to dissolve or re-disperse. Most commercially available powder does not readily dissolve and are generally greater than 100 microns. None of the powders tested substantially increased in density when water was administered. For this reason, spray dried WC powder was made using a pilot production spray dryer unit. This increased vertical integration of the 3DP process facilitated optimal end-product control through a direct improvement in the properties of the powder bed.

5.1 TUNGSTEN CARBIDE SPRAY DRIED POWDER

5.1.1 Niro Spray Drying

A centrifugal atomization method was used to make spray dried powder for 3DP. The atomizer manufacturer is Niro of Denmark. Slurry was ported into a wheel rotating at 15,000 rpm. The impetus for the rotating atomizer wheel was impinging compressed air regulated at 100 psi. Droplets formed as streams of slurry were spun outward. This method of atomization is most commonly used in cases where relatively fine powders (mean particle diameter 30 to 100 microns) are required or in very large systems [Shaw].

Aqueous WC slurry with 1.8 d.w.p. Duramax 3007 slurry was delivered to the unit. The first experimental run was with a slip consisting of 30 v/o (86 mass percent) while the second run slip consisted of 40 v/o WC (91 mass percent). A MasterFlex peristaltic pump was used with minimal fluid line lengths. Figure 5.1 shows typical pump mass flow rates at various settings. During spray dryer operation the mass flow rate into the spray dryer unit should be kept below 100 grams per minute, otherwise, slurry is certain to land wet on the walls. When the unit was opened for cleaning, a one-half inch diameter cross section half ring was found around the entire internal diameter of the unit.

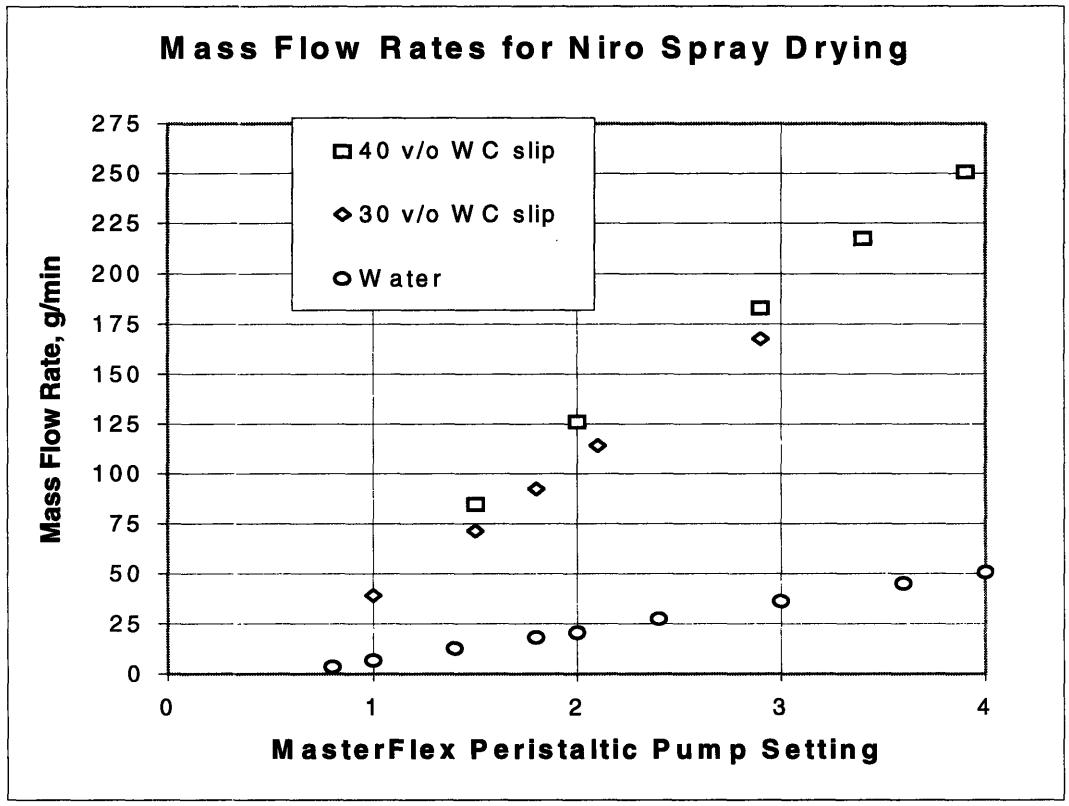

Figure 5.1 -- MasterFlex Pump Settings for Niro Spray Drying

Water is given for reference only and was not spray dried, per se.

Toxicity and contamination issues precluded the introduction of cobalt into the spray dryer unit. The 50% powder yield was far from optimal and Niro staff stated that yields in excess of 90% have been obtained with this pilot unit. The yield was as a result of slurry that landed wet on the spray dryer wall. Figure 5.2 shows a scanning electron micrograph of the powder produced from the first run before classification. The size distribution of the powder collected is shown in Figure 5.3. A sieve shaker was used to classify the powder.

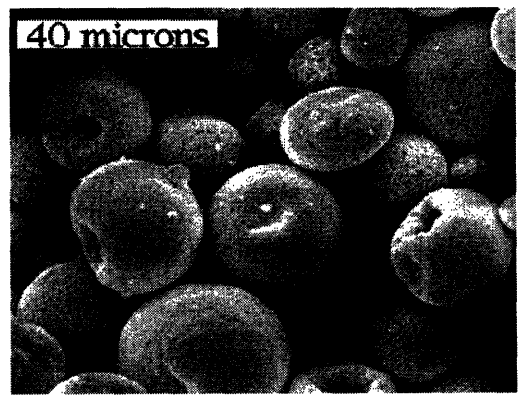

Figure 5.2 -- 38-53 micron Niro Spray Dried WC

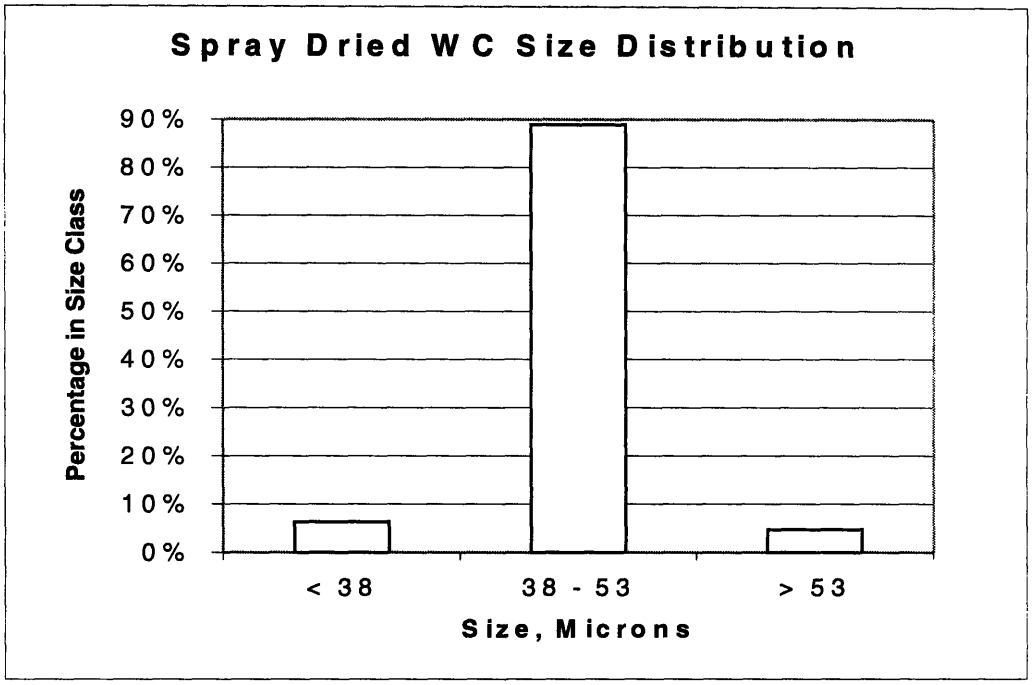

Figure 5.3 – Spray Dried WC Powder Size Distribution. Niro First Run.

5.1.2 Internal Pellet Porosity

Administering a drop of water to a thin layer of particles on a glass slide makes it easy to separate a small amount of hollow and solid pellets. Hollow pellets float due to surface tension, typically, with the void opening pointing upward. Denser solid pellets or pellets with small internal voids tend to sink.

Another method to qualitatively determine the frequency of hollow pellets is to pour a small amount of powder into alcohol. The pellets are not soluble in alcohol and evolved air may be seen escaping from the pellets with the naked eye.

Attention was also given to the distinction between possible large hollows inside the spray dried pellets versus the uniform small void porosity of the pellet shell. Suppose a large internal void comprises a significant amount, say 50%, of the overall porosity of a single spray dried pellet. See Figure 5.4. Then for a 50 micron spray dried pellet, assuming that the shell of the particle is 50% dense, the internal void would have to be 26 microns. This is much smaller than the voids actually seen when large droplets are administered to the bed as shown in Figure 5.5. Altogether, it is still not known whether

this type of internal pellet void or interparticle porosity is the main contributor to the overall large porosity.

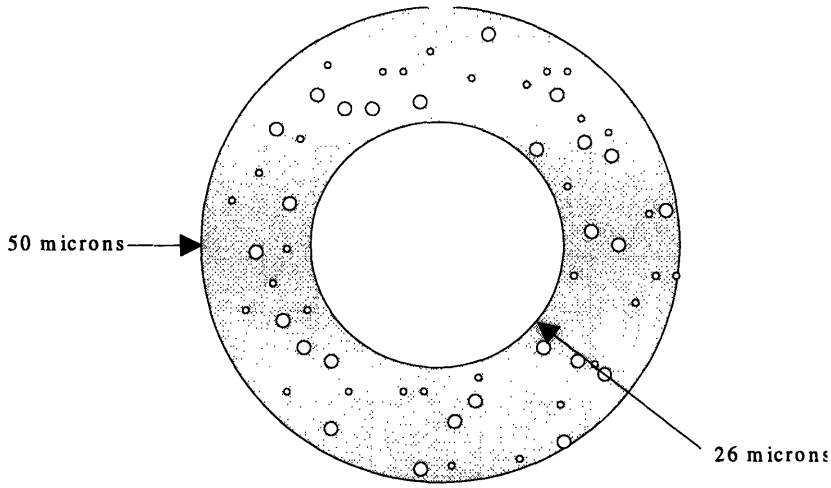

Figure 5.4 -- Cross-Section of a Spray Dried WC Pellet

Large void comprises 50% of porosity. Figure is to scale.

5.1.3 Single Primitive Defects

Single primitives were made by administering a droplet of water to the powder bed through a 152 micron nozzle affixed to a syringe. Figure 5.5 shows a fractograph of one of these primitives. Note that the top of the primitive was dimpled due to ballistic ejection of the individual spray dried pellets.

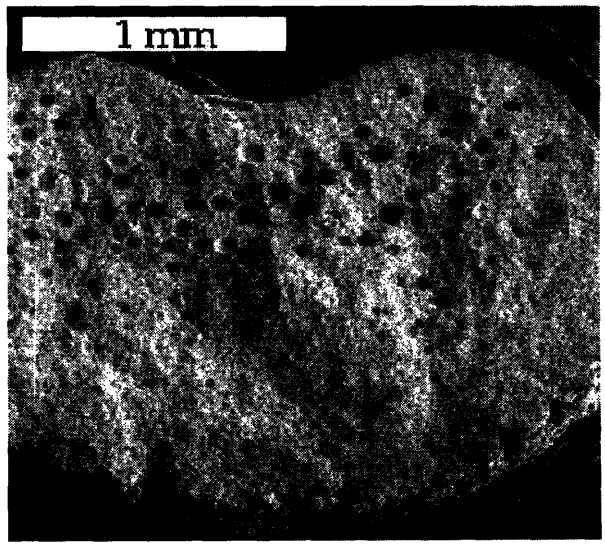

Figure 5.5 -- 38-53 micron Niro Spray Dried WC Primitive

A single droplet of water was administered to the powder bed through a 152 micron nozzle.

Eighty micron internal voids were detected in fractographs of pellets made by syringe dispensed droplets. See Figure 5.6. The syringe was affixed to a 152 micron nozzle and water was administered to the bed. It was deduced that the accumulation of a number of air bubbles produced these defects. The fact that there were many obviously hollow pellets in the first run prompted Niro spray dryer benchmarking and a designed experiment to improve powder quality.

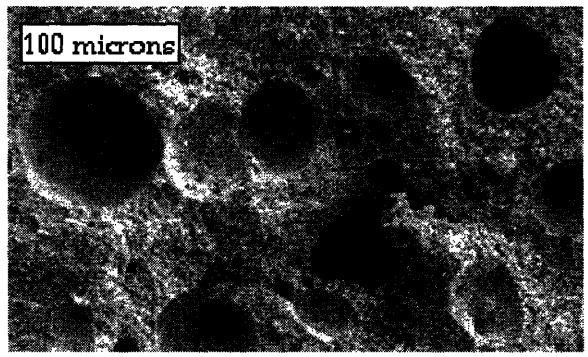

Figure 5.6 -- Large Internal Porosity in 38-53 micron Niro Spray Dried WC Primitive

5.2 SOLID SPRAY DRIED PELLETS

Commercially available spray dried powder is usually hollow and/or dimpled like the powder that was produced in the first run. In addition, many of the pellets produced from the first run of the Niro atomizer were also hollow. Hollow pellets form because, during evaporation, liquid in the droplet migrates to the area of the highest evaporation rate – the outer surface of the droplet. To reiterate, solid spray dried pellets in the powder bed:

1. increase the apparent density of the powder bed, and, hypothetically,
2. retard air bubble accumulation.

To produce solid spray dried powder, a number of variables were considered, including:

1. increasing the slip solids loading from 30 v/o to 40 v/o WC,
2. lowering the inlet drying temperatures to slow drying,
3. varying the slurry feed rate,
4. reducing the amount of deflocculants, binders, solubles, and,
5. changing the atomizer speed.

Items 1, 2, and 3 were chosen and implemented simultaneously on the recommendation of Niro. An increase in the solids loading of the slip was known to increase pellet size. The second run powder was indeed larger than the first run. Varying the mass flow rate of the feed stock had no effect on the packing fraction of the powder. The literature reports that varying the mass feed rate may be used to control the exit temperature. The temperature decreased only 4 degrees Centigrade when the mass flow rate of WC slip was increased from 150 to 220 grams per minute. Item 4 was impractical due to time limitations and the daunting task of developing a suitable slip with a different aqueous formulation. Item 5 was impractical to implement since, as the atomizer speed changes, so does the size of the pellets.

Figure 5.7 shows a scanning electron micrograph of the resulting 53-88 micron spray dried tungsten carbide.

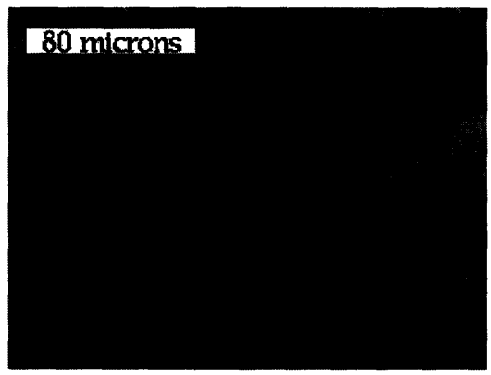

Figure 5.7 -- 53-88 micron Niro Spray Dried WC

Table 5.2 summarizes the powder characteristics for the two different runs of the Niro pilot atomizer. The immediate result was a 7.7% relative increase in the density of the powder bed. Since the powder produced in the first run was highly flowable, the increase in packing fraction could not be attributed to frictional forces alone. Instead, the increase was attributed to a decreased distribution of particles with internal voids. It can be shown that this increase in apparent density is commensurate with that for solid spray dried pellets.

Run	WC Slip Loading	Inlet Temp. (°C)	Apparent Density (g/cc)	Packing Fraction	Size (microns)	$t_{infiltration}$ (seconds)
1	30 v/o	300	3.8	0.26	38-53	1200
2	40 v/o	220	4.2	0.28	53-88	<2

Table 5.1 -- WC Spray Drying Parameters and Results.

Water was administered by syringe through a 152 micron nozzle in both cases. The time for water to infiltrate the larger powder was three orders of magnitude less than that required to infiltrate the smaller powder. Long infiltration times lead to balling when printing lines. For this reason, it would be more desirable to use larger powder *if* it can be made to redisperse.

Figure 5.8 indicates that the 53-88 micron Niro spray dried WC powder does not dissolve appreciably, even at high dosage. In this instance, higher dosage simply means more water. The idea was that, since the powder was known to dissolve when a small amount of it was poured into a beaker of water, it stood to reason, that increasing the amount of water available to redisperse the powder would be beneficial.

Figure 5.8 -- 53-88 micron Niro Spray Dried WC Resists Dissolution at High Dosage
The scale is in millimeters.

In this case, water was administered to the powder through a 3 cc syringe without a nozzle. For comparison, this drop was approximately 270 microliters as compared to a 57 microliters drop made using a 152 micron nozzle. Note the very minor difference in the porosity in the upper middle section of the fractograph as compared with the remainder of the section.

Table 5.2 summarizes the packing fractions of the two different Niro spray dried powders after the administration of a droplet of water through a 152 micron nozzle. Since the primitive packing fraction of the 53-88 micron powder was lower, even though the bulk density of the virgin powder was higher, it was obvious that this powder did not redisperse as well as the 38-53 micron powder. Thus, the bulk of the experiments were confined to the 38-53 micron powder. Still, it might have been possible to successfully carbon dioxide getter this powder using the technique described in Chapter 7.

WC Spray Dried Powder	Apparent Density (g/cc)	Packing fraction (---)
38-53 micron	6.3	0.42
53-88 micron	5.8	0.39

Table 5.2 -- Primitive Packing Fractions for Both Niro Spray Dried Powders

The density was determined by a water displacement (alternative porosimetry) method. Water was administered to the powder through a 152 micron nozzle. The packing fraction corresponds to the apparent density for each case.

6.0 DROP-ON DEMAND BALL PRIMITIVES

6.1 THE EFFICACY OF SMALLER DROPLETS

Duramax hydrophobicity and smaller particle size severely hampered aqueous infiltration into the powder from the first run. This prompted a search for methods to expedite imbibition while ensuring dissolution. Two methods were considered:

1. surfactants, and,
2. smaller droplets.

Details regarding the infiltration search and surfactants tried can be found in APPENDIX C – INFILTRATION SEARCH. Smaller droplets were considered primarily because it was necessary to understand if dissolution still occurs for minimal dosage. In addition, it was generally observed that smaller droplets administered to the bed with a syringe infiltrated more rapidly.

Smaller droplets can be easily made by driving a Hewlett Packard (HP) printer cartridge with an arbitrary waveform generator [Baker]. In addition, the arbitrary wave form generator was programmable allowing for the administration of a discrete number of drops. This was done by modifying the *burst count* in the generator. Single ball primitives of different diameters were made by varying the number of droplets delivered by the cartridge.

The HP cartridge was positioned 2 millimeters away from a level spray dried WC powder bed. HP ink was used initially to debug the electronics and then to provide a control for water experiments. After each administration, the powder bed was manually moved while the cartridge remained fixed. Pellets were immediately collected by sieving. The diameter of each pellet was determined by averaging four pellets randomly chosen under an optical micrograph. Figure 6.1 shows primitives made by administering 1,000 DOD drops of water to the 38-53 micron Niro spray dried WC.

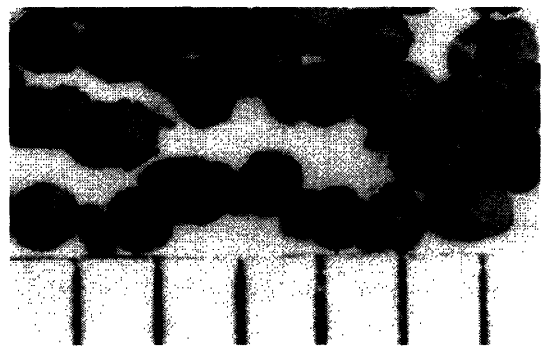

Figure 6.1 -- 800 micron DOD Ball Primitives

1,000 drops of water printed into 38-53 micron Niro spray dried WC. The scale is in millimeters.

Figures 6.2 and Figure 6.3 below show that the 38-53 microns spray dried WC was indeed hollow. The spray dried particles comprising the primitive were clearly eroded on the exterior.

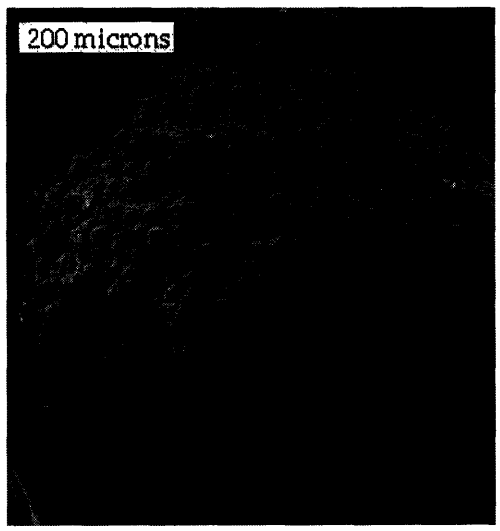

Figure 6.2 -- 500 micron DOD Ball Primitive

Each primitive required 200 DOD water drops.

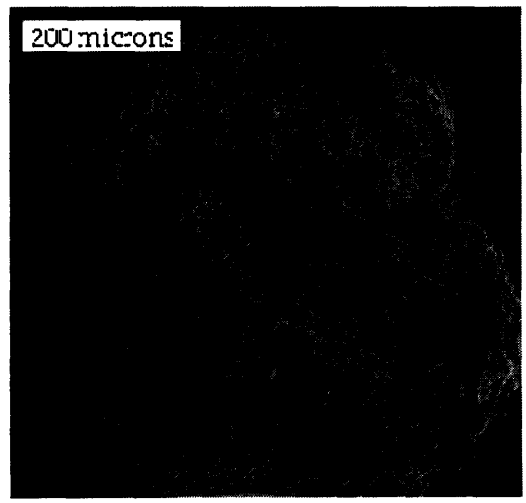

Figure 6.3 -- 500 micron DOD Ball Primitive Fractograph

Each primitive required 200 DOD water drops.

Figure 6.4 shows that the diameter of pellets increases as a cube root of the number of drops. Since the trend obeys a cubic relationship, it can be inferred that the density remains roughly constant for primitives made using 1 to 1000 DOD drops. This is because the diameter is the cube root of the droplet volume which is directly related to the number of drops, N. The ink used was the standard Hewlett Packard black ink. An equation for this relationship was determined by eye. The graphically fitted cube root equation for the primitive diameter, D, was:

$$D = 76\, N^{1/3}.$$

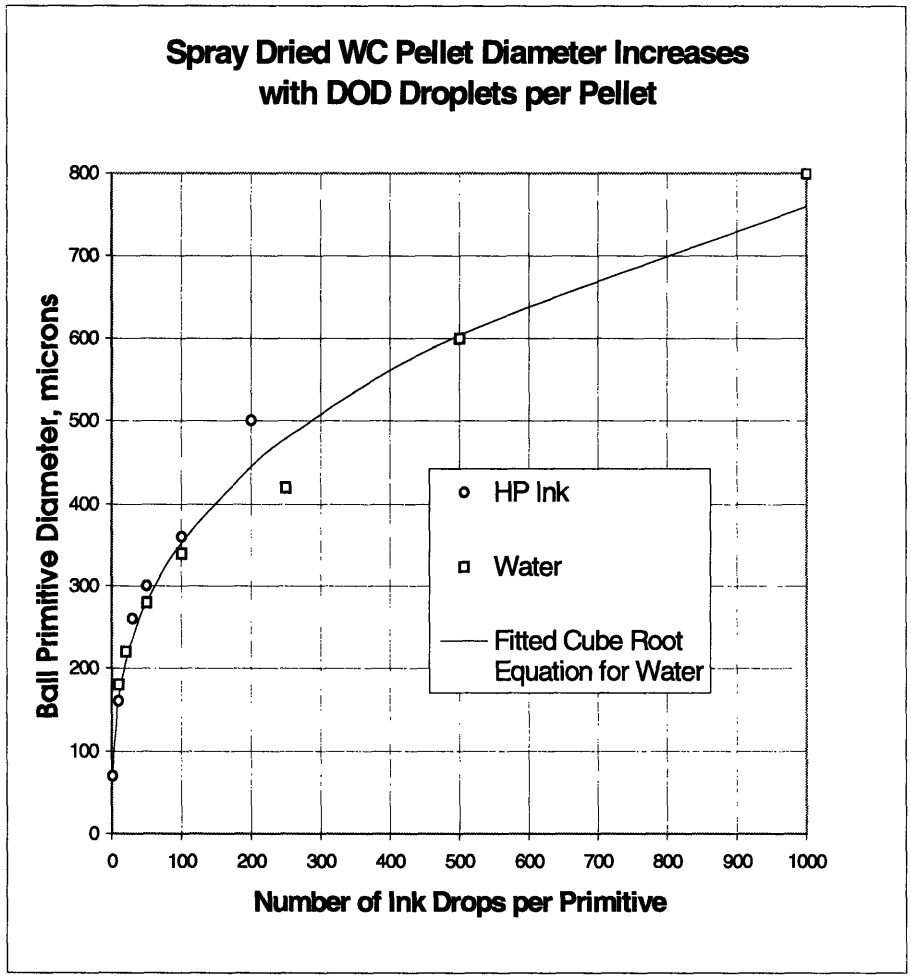

Figure 6.4 -- DOD Ball Primitives Produced Using a HP Cartridge
Water was printed into 38-53 micron Niro spray dried powder.

For reference, it would take 54,000 DOD drops to equal the volume of one 152 microns syringe drop. The Hewlett Packard print head was driven at 3,600 Hz for 15 seconds to produce roughly 54,000 drops in a 38-53 micron spray dried WC bed. These parameters were arrived at by comparing the mass of a 152 micron nozzle droplet and the mass of droplets that were produced by the DOD print cartridge. See Figure 5.9. The primitive was similar to the syringe primitives but exhibited better surface topography due to reduced ballistic ejection. However, the primitive was not spherical like the rest of the DOD primitives. This is likely due to the fact that the gravitational force acting upon a droplet becomes significant as the droplet increases in mass. The largest internal voids in the 54,000 drop primitive were nearly 100 microns. This pellet was compared to the air quench pellets shown in Chapter 8, Figure 8.7 -- Air Quench SEM, 23°C to 0°C.

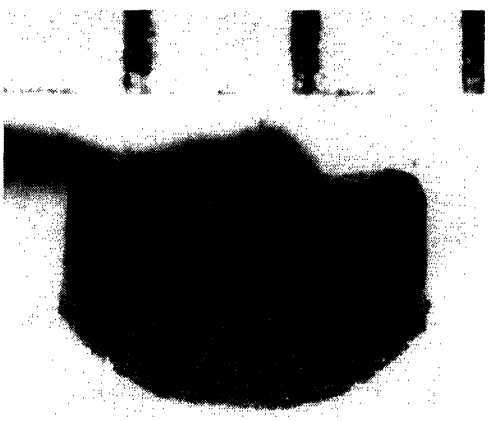

Figure 6.5 -- 54,000 DOD Water Droplets into 38-53 Niro Spray Dried WC

6.2 PRIMITIVE PACKING FRACTION

The resulting packing fraction for the largest of these primitives was ascertained through mercury porosimetry. Small porosity was shown to comprise 20% of the total primitive porosity.

Table 6.1 shows packing fractions for a DOD primitive and a syringe primitive. Water was the infiltrant in both cases.

Administration Method	38-53 micron Niro Spray Dried WC Primitive Packing Fraction
Syringe and 152 micron nozzle	0.47
1000 DOD drops/pellet	0.40

Table 6.1 -- Packing Fractions for Primitives made with a Syringe and a HP Cartridge
Mercury porosimetry was used to calculate the packing fraction in both cases.

6.3 POWDER BED SATURATION

Water saturates a powder bed until capillary pressure and evaporation hinder further liquid migration. The saturation for the DOD primitives was calculated and found to be in good agreement with the hypothesis that liquid tends to migrate through the shells of the spray dried pellets. For the entire range of DOD pellets produced, let

f = packing fraction of 38-53 micron spray dried powder,
D_p = diameter of the dried primitive in microns,
N = number of DOD water drops required to make primitive,
S_{av} = average saturation for all DOD primitives,
V_l = volume of water in a DOD primitive in μm^3, and,
V_g = porous volume within the primitive μm^3.

The volume of a single HP DOD droplet was 110,000 μm^3. Therefore,

$$V_l = (110{,}000\ \mu m^3)(N),$$

while,

$$V_g = \frac{(1-f)(\pi)(D_p)^3}{6}.$$

Also, since,

$$S_{av} = \frac{V_l}{V_g}, \text{ and,}$$

$$D = 76\ N^{1/3},$$

It follows that

$$S_{av} = \frac{(6)(110{,}000\mu m^3)}{(1-0.26)(\pi)(76\mu m)^3}$$

$$S_{av} = 0.65.$$

Although this mean saturation was less than what was typical for solid pellets, saturation levels varied widely. The lowest saturation was 0.46 for the 10 DOD drop primitives. There was a relative maximum saturation of *0.96* for the 250 DOD drop primitives. The neighborhood of 250 DOD droplets per primitive might represent an important regime since, at this point, there would be very little entrapped gas in the wet primitive. Figure 6.5 gives the saturation curve. Note that powder bed saturation levels of 0.8 or greater are not uncommon in 3DP.

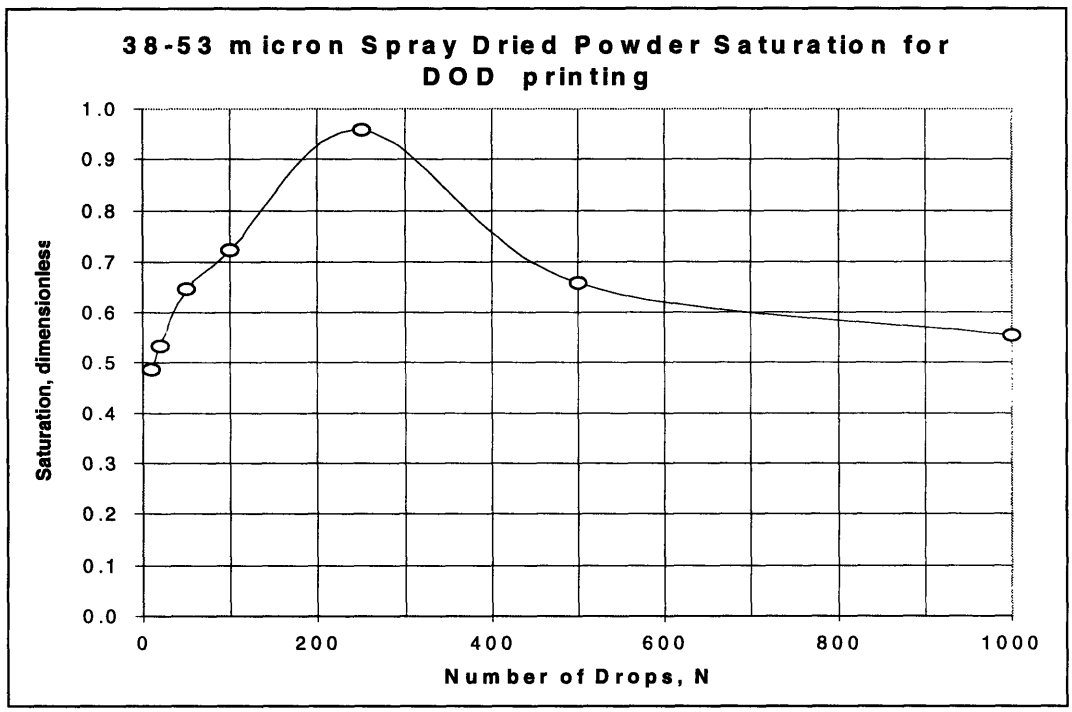

Figure 6.6 -- Saturation Data for 38-53 micron DOD Primitives

Strictly speaking, the porosity in the powder bed was not the same as the porosity in the pellets after the powder had rearranged. Rearrangement of the powder reduced porosity. Recall that

$$f = 1 - \text{porosity}.$$

Therefore, the appropriate value of f might have been slightly higher than the packing fraction of the bed, 0.26. However, f could not have been as high as 0.40, the packing fraction of the completely rearranged primitive. That would have implied a saturation greater than unity in at least one case. This final analysis of the powder bed saturation should be taken with a grain of salt due to the noise level of the measurements taken.

7.0 CARBON DIOXIDE GETTERING

7.1 ENTRAPPED AIR

As mentioned in Chapter 5, spray dried particles may have large and small internal porosity. Gas evolved from spray dried tungsten carbide powder poured into alcohol. This evolution could be seen with the naked eye. Gas evolution was also observed when single droplets of water were administered to a powder bed. This evolution was observed through an optical micrograph. As the hemispherical dome of water sat atop the powder bed, gas bubbles could be seen rising to the top of the droplet. The driving force for bubble ascension was the elevation head within the droplet.

There were never any large pores observed on the top surface of primitives. Large gas pockets that coalesced could have risen within the primitive, however, these pockets almost always lacked the energy to break the surface. Smaller gas pockets might never have coalesced. These smaller voids would be responsible for those observed in the middle to lower sections of the final primitive. Refer to Figure 8.7.

It was observed that the large porosity in primitives was always on the order of he size of the powder. In some instances, individual pellets could be seen and the large porosity was clearly the result of either, a hollow spray dried pellet or the result of a void between spray dried pellets. Once evaporation was complete, these pores remain unfilled by WC and became sites for entrapped air. Further, these sights decreased the packing fraction of the resulting primitive. It was hypothesized that, if these entrapped air pockets could be removed, then the resulting primitive packing fraction could be made to approach that of a slip casting, 0.52.

Administering degassed water to a powder bed under vacuum tested this hypothesis. A vacuum pump was used to maintain the pressure inside of a dessicator above the saturation pressure of water at room temperature. Typically, the lowest vacuums pulled were 25 to 40 torr. Thereafter, a single 50 micro-liter droplet was dispensed into the 38-53 micron Niro spray dried WC. Various times were allowed to elapse before the

dessicator was vented to atmospheric pressure. The elapsed times allowed were 30 and 60 seconds, 2 and 10 minutes. All experiments were carried out at 24°C.

Fractographs revealed that the primitives made in this fashion were virtually free of large defects. However, for the shorter times, small defects were observed at the bottom of the primitive. This suggested that at least 2 minutes was required for water to infiltrate, entrap gas and dissolve the spray dried pellets. Note that up to 20 minutes was still required for complete drying once each primitive was removed from the dessicator.

Figure 7.1 and Figure 7.2 show fractographs of a primitives made when the dessicator was vented to the atmosphere after 30 seconds and 1 minute, respectively. Note the porosity in the lower half of the section. This porosity remained as a result of incomplete enclosure of gas pockets. This entrapment process would be most complete for the upper section of the primitive where there would be more time. The lower section of the primitive did not have enough time for a complete and uniform vapor barrier to form and enclose gas. Gas leakage paths to the outside of the primitive resulted in porosity once drying was completed.

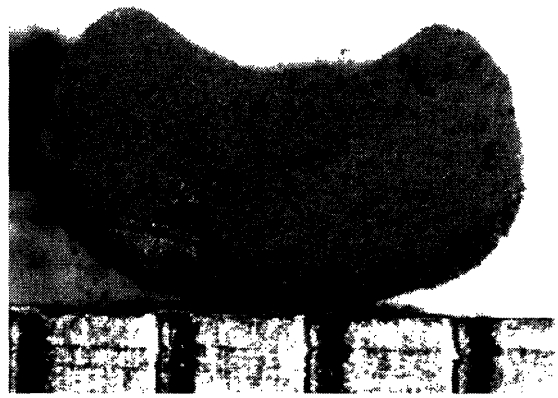

Figure 7.1 -- Fractograph of a Thirty Second En Vacuo Spray Dried WC Primitive
Dessicator was vented to the atmosphere after 30 seconds. The marker is in millimeters.

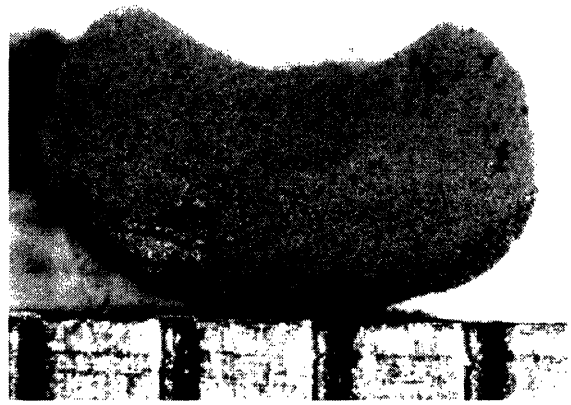

Figure 7.2 -- Fractograph of a One Minute En Vacuo Spray Dried WC Primitive
Dessicator was vented to the atmosphere after 1 minute. The marker is in millimeters.

Figure 7.3 shows a fractograph of a primitive made when the dessicator was vented to the atmosphere after 2 minutes. Note that the concave depression in the upper side of the pellet resulted from some ballistic ejection of the powder at droplet impact. Only in the lowest middle region of the primitive was there any sign of large, approximately 50 micron, porosity. This porosity was attributable to the incomplete surrounding of the primitive volume as previously discussed.

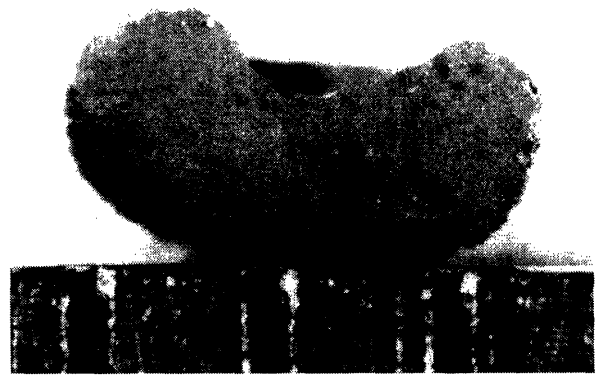

Figure 7.3 -- Fractograph of a Two Minute En Vacuo Spray Dried WC Primitive
Dessicator was vented to the atmosphere after 2 minutes. The marker is in millimeters.

Figure 7.4 shows a fractograph of a primitive made when the dessicator was vented to the atmosphere after 10 minutes.

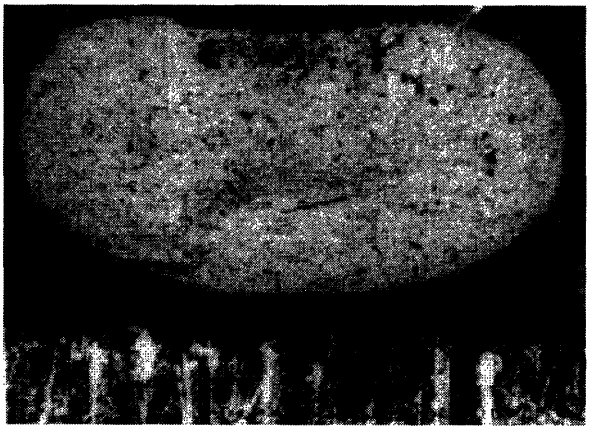

Figure 7.4 -- Fractograph of a Ten Minute En Vacuo Spray Dried WC Primitive
Dessicator was vented to the atmosphere after 10 minutes. The marker is in millimeters.

These experiments conclusively proved that the absence of gas in the powder bed can potentially produce primitives with much smaller flaws and more uniformity. The essential prerequisites were total gas entrapment by pellets which redispersed. Note that it was possible that voids did not form under vacuum. Additionally, these voids might have been collapsed by the pressure transient developed when the dessicator was vented to the atmosphere. Also note that the drying time for primitives internal to the dessicator decreased with increasing residence at low pressure.

7.2 GETTERING THE TRAPPED GAS

Gettering is practiced in metallurgy and semiconductor manufacture to remove contaminants. In this application, carbon dioxide (CO_2) was to be gettered by water to remove the entrapped gas from the powder bed. Carbon dioxide is readily available commercially and the atmosphere contains approximately 340 ppm of carbon dioxide. Although sulfur dioxide has a solubility which is an order of magnitude higher, it is highly noxious and odiferous.

The amount of air comprised by the large porosity in primitives was used to determine how much gas was to be absorbed by the gettering liquid. That is,

$$\frac{Large Porostiy}{TotalPorosity} = \frac{p_{ballprimitive} - p_{slipcasting}}{p_{ballprimative}}$$

where,

$p_{slip\ casting}$ = 0.48, the porosity in the densest slip casting of the WC, and,

$p_{ball\ primitive}$ = 0.60, the porosity in the 1000 DOD drop ball primitives.

And substitution yields,

$$\frac{Large Porostiy}{TotalPorosity} = \frac{0.60 - 0.48}{0.60}$$

Thus, large porosity was shown to comprise approximately 20 % of the overall primitive porosity. At a minimum, this amount of gas must be removed. The volume of gas, V, must cross a surface area, A, in a given time, t, such that the

$$\text{Gettering Absorption Velocity} = \frac{V}{At}$$

The gettering velocity can be related directly to the mean porosity and particle size. Assume that there are n tiny spherical gas pockets after infiltration. Further, assume that all of these pockets are spherical and collectively comprise the gas volume, V, to be removed. The diameter of these pockets will be on the same order as the diameter of the powder. The number of spherical pockets will be

$$n = \frac{6V}{\pi D_p^3}$$

These gas pockets have total surface area,

$$A = n\pi D_p^2,$$

therefore,

$$\text{Absorption Velocity} = \frac{V}{At} = \frac{D_p}{6t}.$$

The gettering absorption velocity required for 60 micron spray dried powder was calculated to be 5 microns per minute for an infiltration time of 2 minutes. See Figure 7.8.

7.3 CARBONIC ACID FORMATION

Carbon dioxide reacts with water to form carbonic acid or bicarbonate:

$$H_2O(liq) + CO_2(g) \rightarrow H_2CO_3(aq)$$

This is an essential step for respiration, photosynthesis and beverage carbonation. Mixers such as tonic water, require high carbonation, using 8.8 g of carbon dioxide per litre of finished product, whereas mineral water fruit drinks may only use 5 g per litre [ICI Australia].

The enzyme carbonic anhydrase consists of about 260 amino acids and has a molecular weight of about 30,000. The enzyme catalyzes carbon dioxide hydration, but catalysis was unnecessary in this case since, as will be seen the initial uptake rate was higher than that required. Furthermore, in the body, the enzyme requires a zinc substrate [Kannan].

7.4 CARBON DIOXIDE SOLUBILITY IN WATER

The literature is rich with information on carbon dioxide and Table 7.1 shows solubility data collected from a number of sources.

Source	Solubility (cc CO_2/cc H_2O)	Temperature (°C)
CRC Handbook	0.822	25
Gerrard	0.935	25
Tinoco et al	0.835	25
Denbigh	0.878	20
Denbigh	0.665	30
Fine et al	0.812	20

Tale 7.1 -- Solubility of Carbon Dioxide in Water at 1 atm

In addition, the solubility of carbon dioxide in water increases with decreasing temperature [Woodruff and Phillips]. Figure 7.5 shows, that by decreasing the temperature of water from 25°C to 5°C, the maximum uptake of carbon dioxide can be nearly doubled.

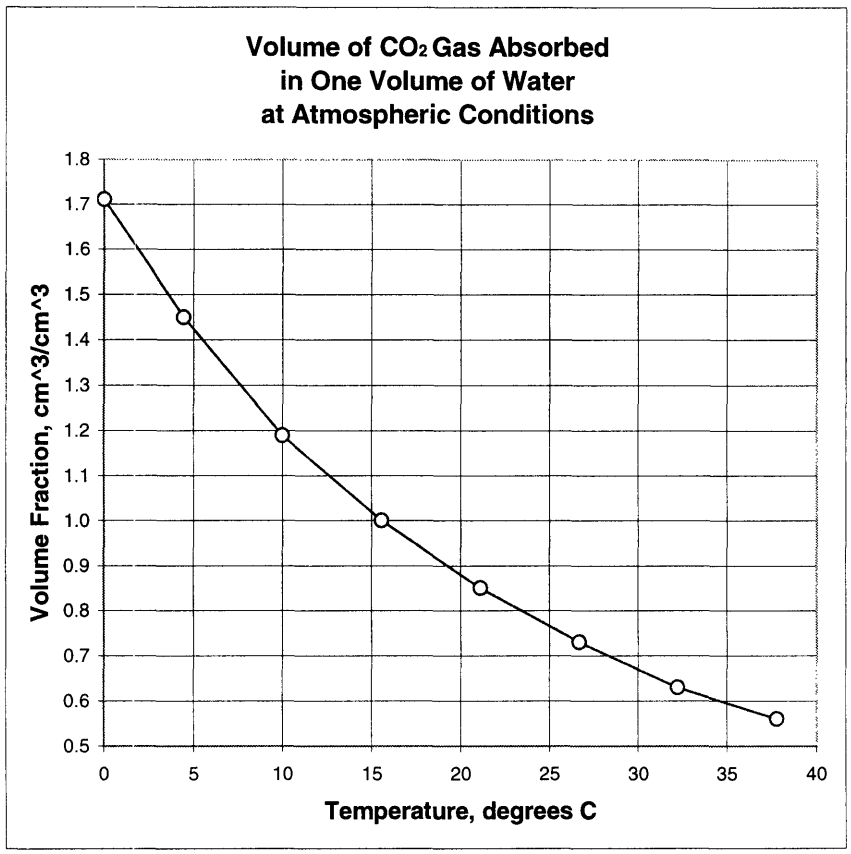

Figure 7.5 -- Temperature Dependence of CO_2 Absorption in Water

7.5 MEASURING CARBON DIOXIDE UPTAKE

An apparatus was developed allowing for the direct calculation of the volume of carbon dioxide absorbed by water at atmospheric pressure. Figure 7.6 shows the gettering experiment apparatus. The design shown allows for uptake measurement at constant atmospheric pressure.

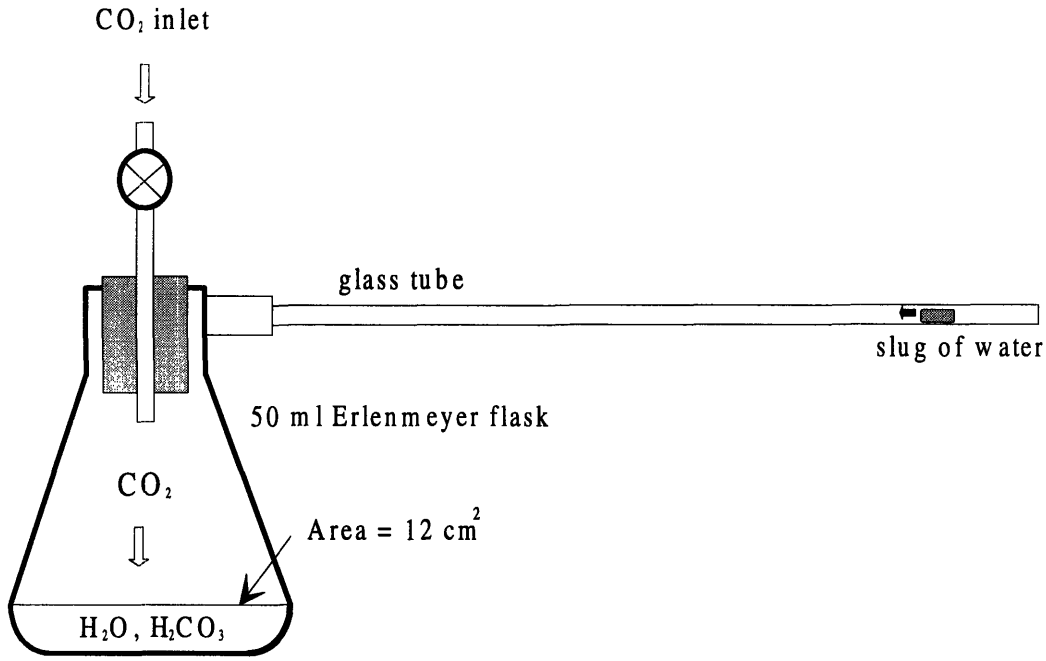

Figure 7.6 -- Gettering Experiment Apparatus
Carbon dioxide hydration removes CO_2, decreases internal gas volume.

In each run, 10 ml of water was placed in a 50 ml Erlenmeyer flask and then degassed or heated. The water was degassed by boiling under vacuum at room temperature. The primary of a pressure regulator was charged while the secondary remained closed. This allowed fifteen volumes of carbon dioxide to flush air from the flask. The secondary on the carbon dioxide tank was then closed. The glass tube was affixed to the flask, then the carbon dioxide inlet nearer to the flask was closed using a hematocrit. A slug of water, which had been previously inserted into the end of the glass tube, was used to monitor the gas volume decrease within the flask. The internal volume of the glass tube was 15.2 cc.

Figure 7.7 shows typical results for carbon dioxide uptake in water. In particular, note that for the degassed water at 23 °C, the total uptake rate is approximately 0.76 cc carbon

dioxide per cc of water after ninety minutes. Compare this with the value obtained from the interpolation of the Woodruff and Phillips data shown in Figure 7.5, that is 0.81 cc carbon dioxide per cc of water. ColorpHast brand pH indicator strips indicated the pH of the water was approximately 4 at the end of absorption. This value for the pH is in agreement with the literature.

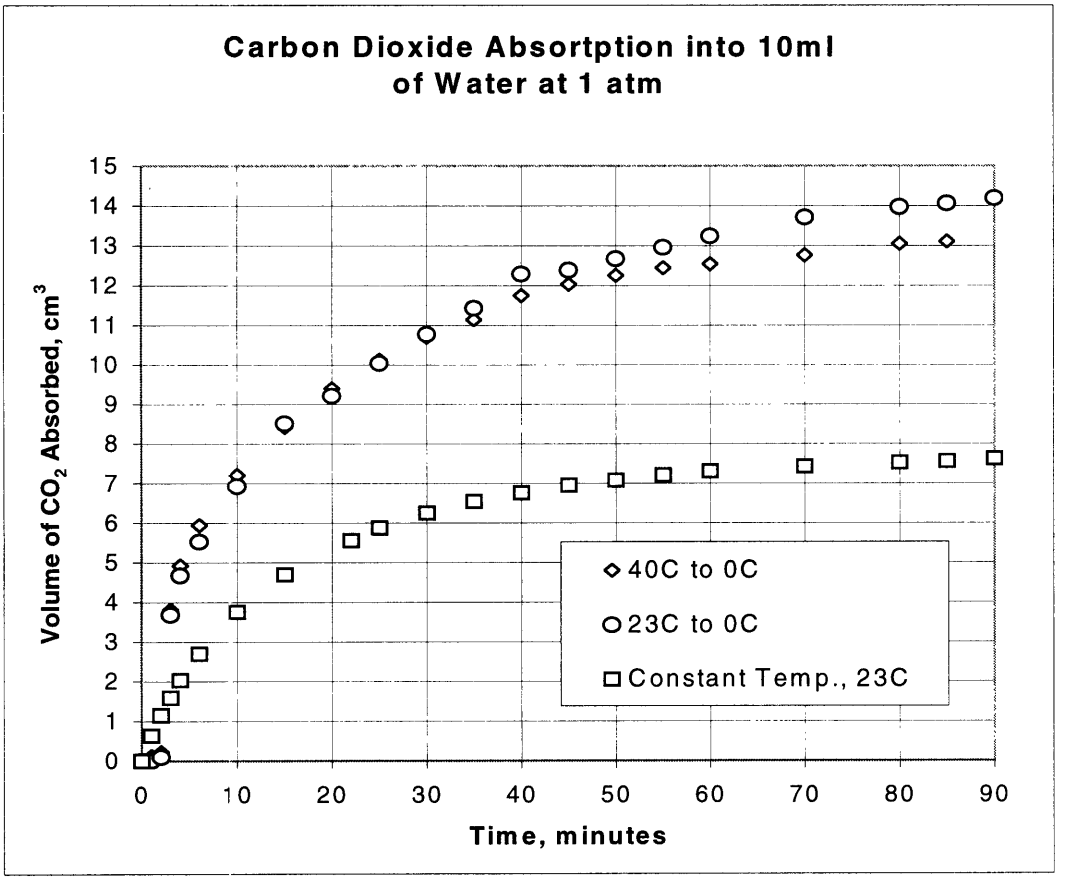

Figure 7.7 -- Quenching Dramatically Increases Carbon Dioxide Uptake in Water
In the constant temperature run, uptake data was recorded immediately after the flask was sealed. In the other two runs, two minutes was allowed to elapse before the sealed flask was immersed in an ice bath. The final temperature of the water inside the flask was 0.4°C.

Note that the above curves slightly overestimate the overall uptake rate. From the ideal gas law, as a gas cools, the volume it occupies decreases. This effect accounts for 8% and 13% of the overall gas shrinkage for the runs which began at 23°C and 40°C, respectively. For the water held at a constant temperature of 23°C the initial absorption velocity was approximately 400 microns per minute. This was calculated by using the last empirical equation in Chapter 7, Section 2.

Figure 7.8 shows typical results for the gettering absorption velocity normalized for the 12 cm^2 surface area of water inside the flask. For experiments in which the temperature was reduced, after two minutes, the sealed flask was immersed in an ice bath to increase the gettering velocity and the overall carbon dioxide uptake. By quenching the water in an ice bath, the gettering rate could be made to increase to 1000 microns per minute. However, the overall uptake increase was the key design parameter that made total porosity removal possible. As will be seen later, increasing the gettering rate does not suffice for removing large porosity.

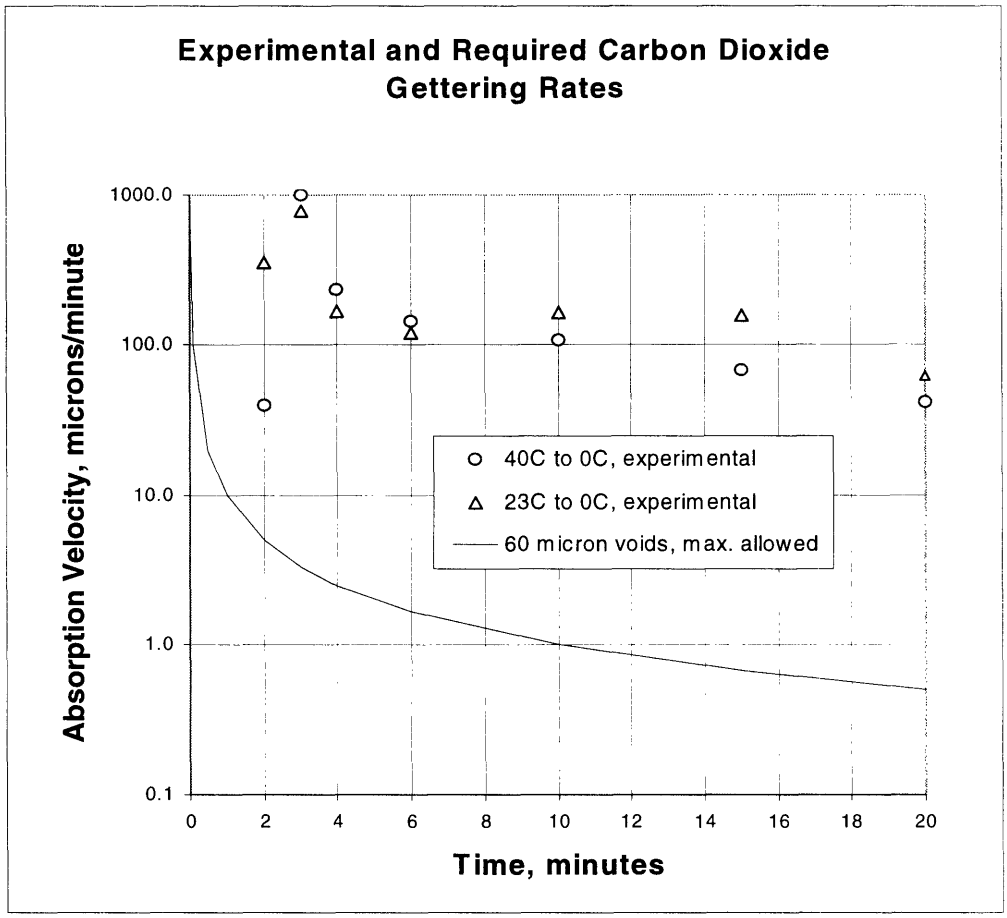

Figure 7.8 -- Carbon Dioxide Gettering Absorption Velocity into Degassed Water

Water was initially at 40°C and 23°C for first and second run, respectively. The water temperature was reduced to 0.4 °C in both cases by immersing the flask in an ice bath two minutes after the run started. The gettering rate is the absorption velocity that would be required to remove the gas from a 60 micron diameter pore in the stated time. For successful gettering to take place, it must take place over a time longer than the redispersion time.

8.0 GETTERING RATE CONTROL DURING INFILTRATION

8.1 GETTERING APPARATUS

The experimentally determined gettering rate was much higher than that actually allowed. Therefore, the water would absorb too much carbon dioxide before sufficient gas was entrapped in the primitive volume. Figure 8.1 shows a primitive that was made by administering water to a powder bed in a carbon dioxide rich environment.

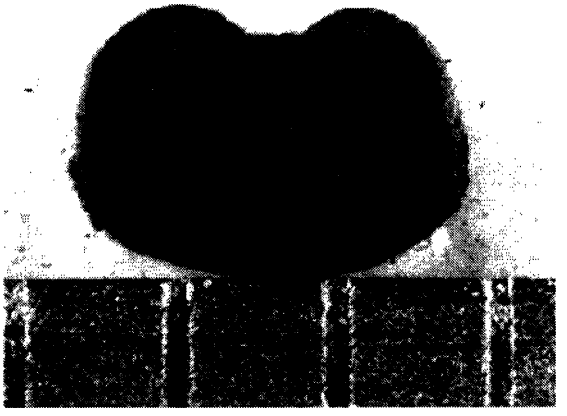

Figure 8.1 -- Primitive without Carbon Dioxide Gettering, Constant Temperature of 23°C
The scale is in millimeters.

Ideally, the liquid should absorb no gas until the liquid has surrounded the gas pockets. Practically, this extreme can be approached by quenching the liquid to increase the overall gas uptake rate. The en vacuo experiments suggested that at least 2 minutes was required for gas entrapment. Thereafter, a rapid absorption of gas by the liquid would be needed to remove gas pockets.

Since the solubility of carbon dioxide decreases dramatically with decreasing water temperature, it was decided that the water should be heated to reduce its initial solubility. In the first experiment, carbonated water was used. Both the spray dried WC and the water to be administered were heated to 40 °C. The powder was contained within a gas tight carbon dioxide rich environment as shown in Figure 8.2.

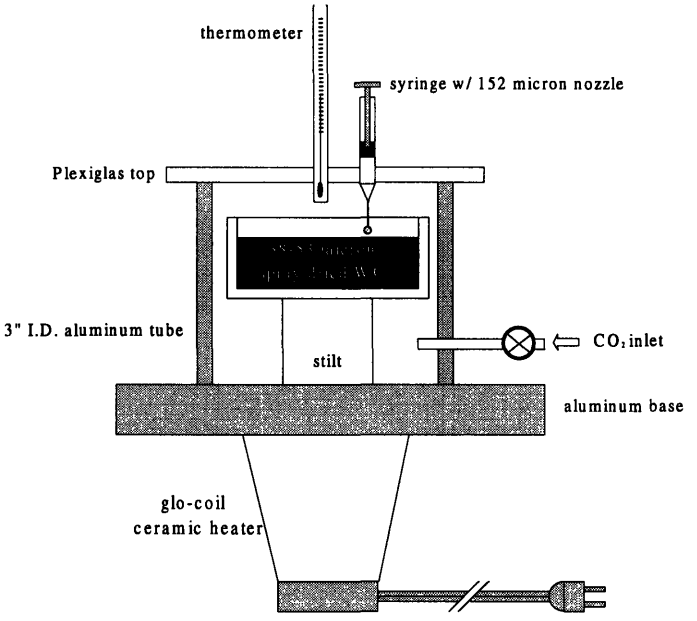

Figure 8.2 -- Carbon Dioxide Gettering Enclosure for Making Primitives
The glo-coil heater was only used when the initial powder temperature was required to be above room temperature.

The syringe could be removed to purge the system of air and fill with carbon dioxide. Note that the syringe was offset from the center so that the Plexiglas top could be spun and a number of primitives could be made at once. After several droplets of water were administered, two minutes were allowed to elapse. The powder bed was then removed from the apparatus and placed in a freezer.

Ultimately, it was determined that heating the powder to 40°C was not necessary. It sufficed to quench the powder from 23°C to remove the entrapped gas. The powder cooled to 0°C in seven minutes and was removed so that the primitive could dry completely. The temperature of the powder was measured by placing a thermometer in the bed. Figure 8.3 and Figure 8.4 show typical fractographs.

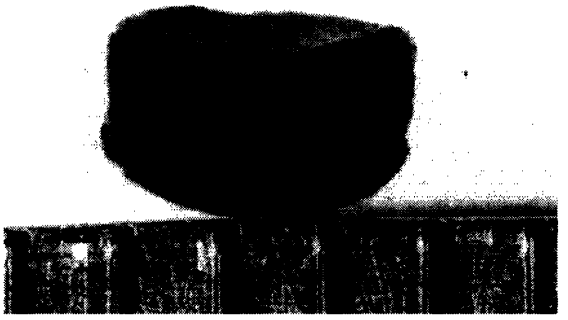

Figure 8.3 -- CO_2 Quench Photograph, 23°C to 0°C
The marker is in millimeters.

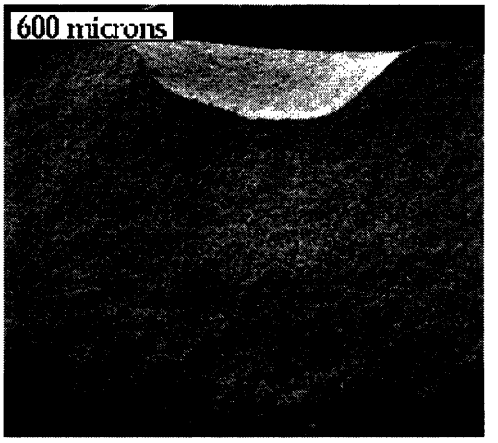

Figure 8.4 -- CO_2 Quench SEM, 23°C to 0°C
50X Magnification

The powder temperature was decreased from room temperature to the 0°C and this nearly sufficed to eliminate all porosity in the middle and upper section of the primitives. Figure 8.5 shows a close up of the lower region shown in Figure 8.3. The largest porosity was 40 microns.

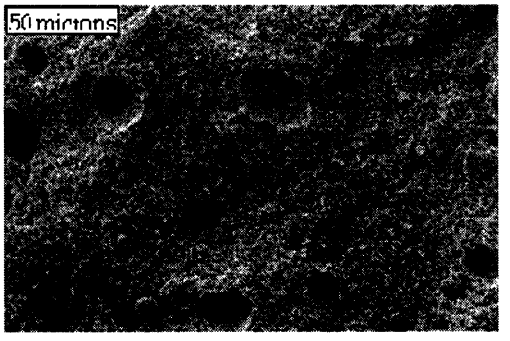

Figure 8.5 -- Close-up of CO_2 Quench SEM shown in Figure 8.3
400X Magnification

Mercury porosimetry revealed that the packing fraction of the carbon dioxide gettered primitives quenched from 23°C to 0°C was, on average, 0.502. This was the average of two different porosimetry runs resulting in packing fractions of 0.487 and 0.516, respectively. The mercury porosimetry data was plotted in Figure 8.6. Notice that the first plateau was very low, almost negligible as a total percentage of the overall porosity. This was indicative of a very low percentage of large porosity in the overall porosity. Plots that had been obtained for slip castings were similar to this one.

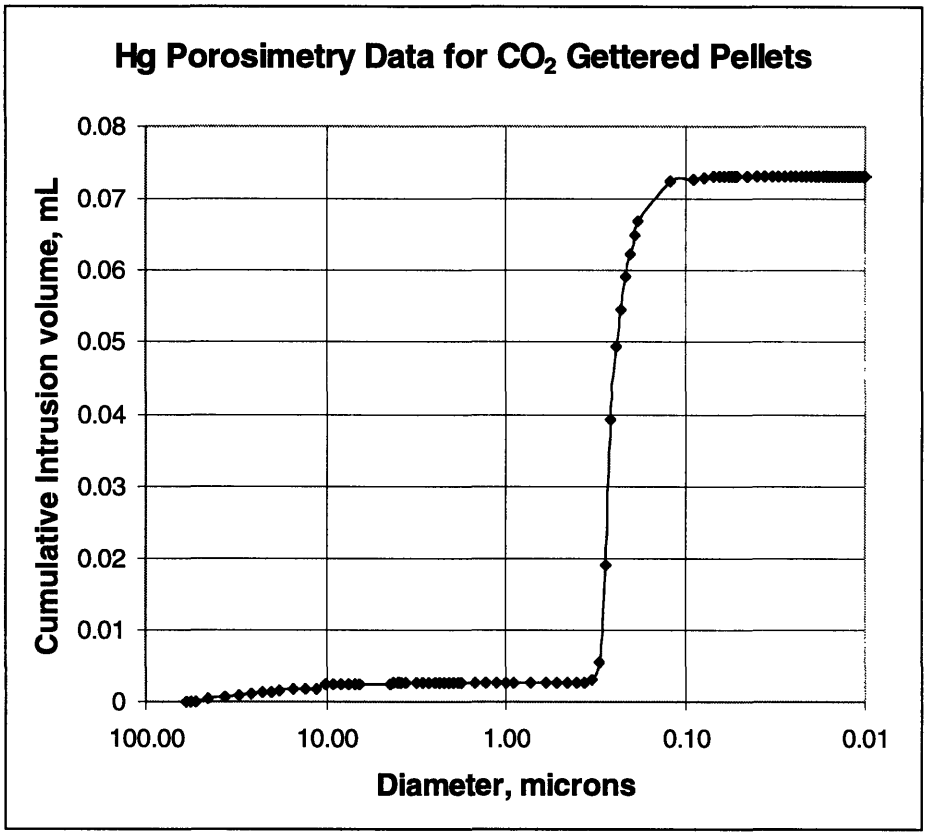

Figure 8.6 -- Porosimetry Data for Carbon Dioxide Gettered 38-53 micron Spray Dried WC

Although these results were very positive, evidently, there was not enough time allowed for infiltration. This could be due to the fact that, in the freezer, where the humidity was very low, drying takes place more rapidly than at ambient conditions. In which case, longer than 2 minutes would be required for complete infiltration and entrapment of gas pockets.

The hypothesis that the infiltration time changed with temperate was further tested by printing cold water into powder and observing the infiltration time. Both the powder and the water were kept at 7°C throughout the experiment. The infiltration time was only 12 minutes. Table 8.1 summarizes infiltration times for the various conditions encountered while administering water to the 38-53 micron spray dried WC. In each instance, both the powder and the water were maintained at a constant temperature throughout infiltration.

Water and Powder Temperature (°C)	$T_{infiltration}$ (minutes)
24	20
40	8
7	12

Table 8.1 -- 38-53 micron spray dried WC Infiltration Time at Constant Temperature

Figure 8.7 shows that merely decreasing the temperature of the water at the outset, as opposed to after infiltration, and allowing the primitive to dry was only successful in gettering the gas in the upper half of the primitive. Evidently, a large amount of carbon dioxide dissolves very rapidly and the water reaches saturation before the gas pockets in the primitive are removed. The accretion of voids in the middle section of the primitive shown substantiates this claim. Note that there are no large voids in the bottom of the primitive since the gas pockets tend to rise.

Figure 8.7 -- 5°C Degassed, Deionized Water into 24°C 38-53 micron Spray Dried WC
The marker is in millimeters.

An additional control experiment was conducted by quenching from room temperature to 0°C except it was carried out under air. Air is, roughly, 78 v/o nitrogen and 21 v/o air with other gases comprising the remaining 1 v/o. The solubility data in Table 8.2 have been calculated from data reported by Gerrard.

Gas	Solubility in Water (cc gas/cc water)
Nitrogen	0.016
Oxygen	0.031
Carbon Dioxide	0.935

Table 8.2 -- Solubilities of N_2, O_2, and CO_2 in Water at 1 atm, 25 °C

The solubilities of nitrogen and oxygen in water are more than an order of magnitude less than the solubility of carbon dioxide in water. It was expected that, relative to carbon dioxide, little air would be absorbed into the water. The resulting fractograph, confirmed that quenching in air had negligible benefit. See Figure 8.8. The porosity within these primitives was also approximately 80 to 100 microns. The packing fraction of these primitives was 0.466 as reported by mercury porosimetry. This packing fraction compared with 0.468 obtained for experiments conducted at a constant temperature of 23°C.

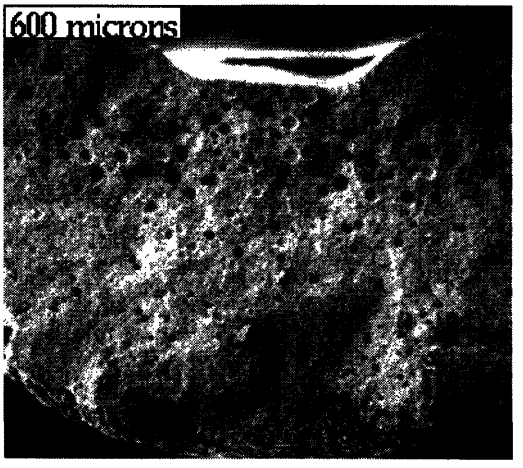

Figure 8.8 -- Air Quench SEM, 23°C to 0°C

It was generally observed that higher dosages resulted in denser and more homogenous cross sections. Note that this was not because smaller droplets absorbed more gas. Although, small droplets with high surface area could potentially absorb gas more rapidly, the water was saturated with carbon dioxide at the outset. The difference between the large and small primitive was the ratio of the external and internal surface areas. The smaller primitive had a larger external surface area through which carbon dioxide could be absorbed. The result was that the water for this drop reached gas saturation before redispersion stopped.

Figure 8.9 shows this phenomenon for powder that was quenched from 40°C to 13 °C under carbon dioxide. Note that even though the temperature differential was larger here, 27°C compared with 23°C in the more successful experiments, the overall carbon dioxide uptake potential was less. Refer to Figure 7.5.

Figure 8.9 -- CO_2 Quench, 40°C to 13 °C
The marker is in millimeters.

8.2 CONTROL SUMMARY

Table 8.3 summarizes the results of the experimental controls. Mercury porosimetry was performed only for a select few of the controls. All of the experiments were performed using the 38-53 Niro spray dried WC. In each case, the packing fraction was determined using mercury porosimetry. These results indicate that, when carbon dioxide gettering was used, quenching in air did not increase the packing fraction relative to a constant room temperature infiltration.

Environment	$T_{initial}$ (°C)	T_{final} (°C)	$t_{infiltration}$ (minutes)	Packing Fraction (---)	Figure
Air	24	24	20	0.468	5.4
Air[1]	40	40	8	---	N/A[4]
Air	7	7	12	---	N/A[4]
Air	23	0	---	0.466	8.8
CO_2[2]	23	23	---	---	8.1
CO_2	23	0	---	0.502	8.3
CO_2[3]	40	13	---	---	8.9

Table 8.3 -- Gettering Control Summary

[1]This fractograph was marginally better than that for the primitives made at constant 24°C.
[2]This was for 5°C water, 23°C WC as indicated in Figure 8.6.
[3]The solubility potential between 40°C and 13°C was not as high as that between 23°C and 0°C.
[4]N/A = Photograph not available at time of printing.

There was large porosity for every experiment except for the quench from 23°C to 0°C. In the lower middle section of those primitive, there was porosity as large as 40 microns. This was a considerable improvement over the 100 micron voids that remain if gettering was not performed.

9.0 CONCLUSIONS

The goal of this work was to apply Three Dimensional Printing to the fabrication of tungsten carbide cobalt parts with a focus on wear parts. Two basic approaches were investigated:

1. Spray dried powder was spread and a highly loaded slurry of tungsten carbide was printed into the powder bed.

2. A special spray dried powder was created which redisperses upon contact with a liquid. In this case the printed "binder" consists simply of a solvent which redisperses the powder bed.

The method wherein a slurry is printed into a bed of spray dried powder did produce green densities which were higher than that of the spray dried powder bed alone. However, the green parts produced by this method had a very significant level of porosity associated with them. Here are several issues associated with this approach. First, whenever a liquid infiltrates a powder bed it migrates past the point of 100% saturation and ends up at some equilibrium saturation which is significantly lower than 100% with the associated porosity in the powder bed (with the associated porosity in the powder bed). Thus, printing highly loaded slurry into solid spherical particles resulted in only about half the increase in green density that might be expected from 100% saturation. Refer to Figure 4.3. A second problem is related to the presence of both large and fine pores in the bed of spray dried powder. An upper bound to the possible green density can be calculated based on the assumption that the liquid vehicle of the slurry fills 100% of both the large and small pores. A lower bound may be estimated under the assumption that the liquid vehicle of the slurry infiltrates only the large pores. Experimental results yield green densities which are intermediate. The conclusion on this portion of the work is that a very delicate balancing act would have to be struck between rates of infiltration

of large and small pores and elimination of porosity associated with fluid migration. Such an approach may be possible, but would at a minimum be quite tricky.

More promising results were obtained along the second path wherein spray dried powder is created which redisperses upon contact of a liquid vehicle. Spray dried powder was fabricated in house using only the powder, water and a dispersing agent. The dispersing agent therefore acted as a binder for the spray dried powder. This spray dried powder was found to substantially redisperse upon contact with water. Primitives were made by dropping a small 57 microliter drop of water into a bed of this spray dried powder. The result was the formation of a primitive approximately 2 mm in extent which showed clear evidence of the redispersion of the spray dried powder and which had typical green densities of 47%. Refer to Figure 5.5. However, there were a significant quantity of fairly large pores evident in these primitives especially near the top portion of the primitives. These pores ranged in size from 30 microns to 80 microns. The hypothesis is that these pores are the result of air trapped during the redispersion and drying process. The air could originate from either or both the air between the spray dried particles or the air within the spray dried particles including within hollow spray dried particles. Further evidence for this hypothesis is the visual observation that as the drop of water penetrates into the bed of spray dried powder, bubbles can be seen rising to the top and popping. The presumption, therefore, is that the trapped pores represent bubbles which were unable to rise to the surface and escape.

In order to test the hypothesis that the voids are the result of trapped gas, primitives were made by dropping water into a bed of spray dried powder under partial vacuum conditions. The vacuum was maintained at a typical pressure of 25 torr to 40 torr as the drop of water was administered to the powder bed (lower pressures would have resulted in the boiling of the water) after different time intervals ranging from 30 seconds to 10 minutes, air was readmitted to the chamber up to 1 atmosphere. The resulting primitives showed a near absence of large pores. Refer to Figure 7.4. We cannot be certain of the mechanism that resulted in this success. It may be that without air present during the

redispersion that pores never form. It may also be that some pores do form but that they collapse when the atmosphere is readmitted and the pellets subjected to the resulting hydrostatic stress. In any event this series of experiments demonstrated that the pores are most likely due to trapped gas and that these pores could be eliminated from the process.

While it is conceivable that 3D Printing could be practiced under a moderate vacuum, it may prove to be quite challenging and an atmospheric pressure alternative was sought. The concept pursued was to absorb the trapped gas into the liquid of the "binder". This is essentially a form of "gettering" where the impurity to be gettered is the gas trapped in the voids. The model system used was the absorption of carbon dioxide into water, recognizing that at room temperature almost 1 cc of carbon dioxide can be absorbed into each cc of water and that the absorption limit goes up as the temperature goes down. An experiment was performed where a drop of water was administered to a bed of redispersable powder under a CO_2 environment. The resulting primitive showed no improvement over primitives made in air. Refer to figure 8.1. Separate experiments sought to verify the absorption limits for CO_2 and water found in the literature and to measure the rate of absorption expressed as a velocity of absorption. The velocity absorption can be calculated by measuring the volume of gas absorbed per unit time per unit area of contact with the liquid. The absorption velocity for CO_2 in water was found to be on the order of 400 microns per minute. At this rate, the gas trapped in a 60 micron pore would be fully absorbed in approximately 0.03 minutes. However, it is very likely that the pores are not yet formed within this time interval. Indeed, for the gettering concept to work, the pores must be fully formed and closed. The walls of the pores must consist only of the fine particles of powder with no larger holes. Only then can the capillary pressure associated with this fine porosity withstand the suction created by the gettering and allow the pore to collapse. If there is a larger opening into the pore, gas can simply enter the pore by that route. Thus, it seems likely that the absorption rate of CO_2 into water is too fast to allow it to getter in the simple case of dropping water into powder under a CO_2 environment.

In order to "switch" the gettering on at the right time, a modified procedure was used. A drop of water was dropped onto the powder under a CO_2 blanket at room temperature. After a few minutes, (presumably enough time for redispersion to take place and for the pores of the trapped gas to form) the entire powder bed was placed in a freezer and the temperature dropped. As noted previously, the absorption limit of CO_2 in water goes up as the temperature goes down in fact it roughly doubles from room temperature to 0°C. Thus, dropping the temperature of the powder bed acts as a switch to turn on the CO_2 gettering operation. Primitives produced by this technique demonstrated a near absence of the large porosity and a green density of approximately 50%, comparable to the green density of slip cast bodies formed in the same powder and dispersant. Refer to Figure 8.4. Some minor porosity was still evident toward the bottom of the primitives. Hypothetically this might be due to the fact that at the periphery, and especially at the bottom, this saturation of water in the powder bed is lower and therefore the redispersion may have been incomplete.

Several controls were also performed. Most importantly, the same process was performed with the powder bed in air. That is, a drop of water was dropped onto a bed of redispersable spray dried powder in air at room temperature and this bed was then transferred after a two minute interval to the freezer. The resulting primitives had green densities comparable to those made by simply dropping water into spray dried powder and air and letting it dry. The porosity in these primitives ranged from was 30 to 80 microns. Refer to Figure 8.8.

In summary, high green density tungsten carbide powders can be fabricated from spray dried primitives under the following two conditions:

1. that redispersable spray dried powder is utilized, and,
2. that voids due to trapped gas are avoided or eliminated (one method of doing so is to getter the trapped gas into the liquid).

This fundamental processing approach has great promise for 3D Printing as it has the potential to produce a very high rate and reliable process. The trapped gas might be gettered either after each layer or after the entire part has been defined. There may be some limitations to the feature size and dimensional control possible by this route and these matters should be among those examined in future work. An additional significant issue for future work to consider is that there is substantial shrinkage associated with the redispersion process and in order to avoid cracking, this shrinkage would have to in general be accommodated vertically.

REFERENCES

Adamson, A.W. (1960). Physical Chemistry of Surfaces. New York: Interscience.

Ashurst. A. & Klar E. "Mercury Porosimetry." ASM Handbook. Vol. 7. 9th ed. pp. 266-271.

Baker, P. J. (1997). Three Dimensional Printing with Fine Metal Powders. M.S. thesis, Massachusetts Institute of Technology.

Benjamin, M.L. (1983) Process for Producing Refractory Powder. US. Patent 4,397,889.

Benjamin, M.L. (1984) Process for Producing Refractory Powder. US. Patent 4,456,484.

Benjamin, M.L. (1984) Process for Producing Refractory Powder. US. Patent 4,478,888.

Bredt, J.F. (1995). Binder Stability and Powder\Binder Interaction in Three Dimensional Printing. Ph.D. thesis, Massachusetts Institute of Technology.

Butler, J.N. (1982). Carbon Dioxide Equilibria and Their Applications. Addison-Wesley: Reading, MA.

Caradonna, M. (1997). The Fabrication of High Packing Density Ceramic Powder Beds for the Three Dimensional Printing Process. M.S. thesis, Massachusetts Institute of Technology.

Fine, L.W. and Beall H. (1990). Chemistry for Engineers and Scientists. Philadelphia: Saunders College.

Friederichs, J. (1997). Internal communication on 9/9.

Guo, R. and Sachs, E. (1993). Modeling, Optimization and Control of Spatial Uniformity in Manufacturing Processes. In IEEE Transactions on Semiconductor Manufacturing (pp. 41-57). Vol. 6, No. 1.

Heinzl, J. (1985). "Ink-Jet Printing." Advances in Electronics and Electron Physics, Vol. 65.

ICI Australia Limited. (1997) "Carbon Dioxide Chemical Fact Sheet." ASN 004 145 868. http://www.ici.com.au/resource/chemfact/carbondi.htm.

Kannan, K.K. (1980) "Crystal Structure of Carbonic Anhydrase." In Biophysics and Physiology of Carbon Dioxide: Symposium Held at University of Regensbur (FRG) April 17-20, 1979. Springer-Verlag: New York. pp. 104.

Mills, K. Ed. (1984). "Production of Tungsten, Molybdenum and Carbide Powders." ASM Handbook. Vol. 7. 9th ed. pp. 152-158.

Phadke, M. S. (1989). Quality Engineering Using Robust Design. New Jersey: Prentice Hall.

Sachs, E., Cima, M., Williams, P., Brancazio, D., and Cornie, J. (1990). "Three Dimensional Printing: Rapid Tooling and Prototypes Directly From a CAD Model." Journal of Engineering for Industry, p. 13.

Schmidt, S.R. and Launsby R.G. (1994). Understanding Industrial Designed Experiments. Colorado: Air Academy Press.

Shaw, F.V. (1990). Spray Drying: A Traditional Process for Advanced Applications. Ceramics Bulletin. Vol. 69. No. 9. pp. 1484-1489.

Shaw, F.V. and Andrews, M.H. (1997). "Spray Drying" in Weimer, A.W. Ed. Carbide, Nitride and Boride Materials Synthesis and Processing. New York: Chapman & Hall.

Smith, G. (June, 1993). Operating the Spray Dryer. Ceramic Industry. p 54-56.

Suh, Chryssolouris, Gutowski, Sachs and Cook. (1990). Manufacturing Engineering. Cambridge, MA. Massachusetts Institute of Technology.

Tinoco, I., Sauer, K., Wang J.C. (1995). Physical Chemistry. New Jersey: Prentice Hall.

Woodroof, J.G. and Phillips, G.F. (1974). Beverages: Carbonated and Noncarbonated. Connecticut: AVI.

APPENDIX A – INFILTRATION OF POROUS PELLETS

A.1 MAKING PRIMITIVES

Project research began with the continuance down a path of work begun by Caradonna. The path approach consisted of printing slurry into porous spray dried powder. Figure A.1 shows a picture of aqueous 25 v/o WC, 1.8 d.w.p. Duramax 3007 infiltrating the 200 micron PEG spray dried WC/Co. The slurry was administered through a nozzle affixed to a syringe. Twenty-five volume percent was the maximum aqueous solids loading that could be made to infiltrate this powder. Note the large porosity that resulted from partial saturation and/or entrapped air in the powder bed.

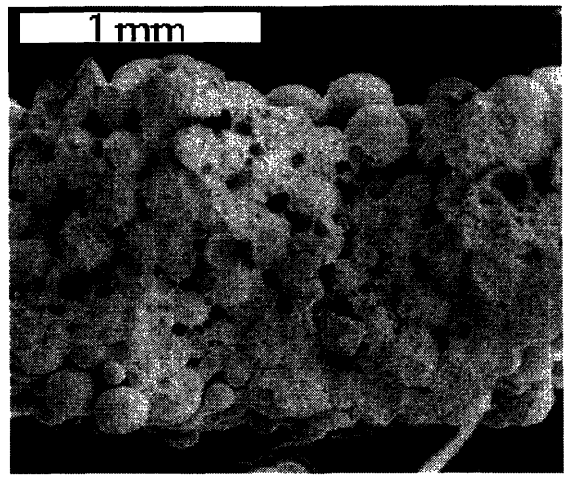

Figure A.1 -- Single Primitive from Aqueous 25 v/o WC, 1.8 d.wp. Duramax 3007 into PEG Spray Dried WC/Co

Measuring the slurry infiltration time into a powder bed is a non-trivial task. Isolating the infiltration constants for interparticle pores and internal pellet voids would be difficult. Nevertheless, an upper and lower bound can be established given certain simplifying assumptions. Let

f_p = packing fraction of an individual spray dried pellet
f_b = packing fraction of spray dried pellets in a bed as though they were solid
s = volume fraction of slurry
t_1 = time required for large pore infiltration
t_2 = time required for small pore infiltration

Then, if

$$t_1 << t_2$$

It must be that

$$f_{lower} = f_p f_b + s(1-f_b).$$

The term in parentheses represents the bed porosity as comprised of the pores between the spray dried pellets. These are interparticle pores. See Chapter 2.6. Also, if

$$t_1 >> t_2$$

It must be that

$$f_{upper} = f_p f_b + s(1- f_p f_b).$$

The term in parentheses represents the bed porosity as comprised of the interparticle pores and the internal pellet voids, i.e., the total bed porosity. See Chapter 2.5. Note that the first term in the upper bound equation, $f_p f_b$, is simply the overall packing fraction of the spray dried powder bed. For 300 micron PEG SD WC/Co the apparent density is 0.26. This insight obviates the need to determine the both f_p and f_b directly.

For illustration purposes, the calculation of the lower and upper bound is presented. Suppose that 25 v/o slurry is printed into a 300 micron PEG SD WC/Co spray dried powder bed. Then,

$$f_{lower} = f_p f_b + s(1-f_b)$$

$$f_{lower} = 0.26 + (0.25)[1 - 0.5]$$

$$\boxed{f_{lower} = 0.38.}$$

And,

$$f_{upper} = f_p f_b + s(1- f_p f_b).$$

$$f_{upper} = 0.26 + (0.25)[1 - 0.26]$$

$$\boxed{f_{upper} = 0.45.}$$

Mercury porosimetry revealed that the actual primitive packing fraction was 0.41, nearly equidistant between the upper and lower bounds. Therefore, the assumptions for the upper and lower bounds seemed justified. Furthermore, the logical was that, to some degree, there was infiltration of both the large and small porosity in the bed of spray dried WC/Co.

A.2 PRINTING LINES

Even though many difficulties were encountered during making primitives, some lines were made. The spray dried powder was supplied by Osram Sylvania. Figure A.2 shows a typical result. Notice that the spray dried powder did not dissolve to any appreciable degree. All of the lines produced in this fashion were riddled with large porosity that was clearly visible to the naked eye.

Figure A.2 -- Lines from Aqueous 25 v/o WC, 1.8 d.w.p. Duramax 3007 Printed into PEG Spray Dried WC/Co

The scale is in millimeters.

Balling was one of the largest impediments to forming complete lines. After the slurry was printed into the powder bed, in a matter of seconds, the printed lines began to contract and from individual cylinders. In the extreme, capillary pressure tended to force the printed lines into spherical balls.

Ballistic ejection was another comp0lication. As slurry entered the powder bed, it tended to make a trench. The walls of the trench would then collapse and often rejoin at the top. This mechanism lead to the large porosity in Figure A.3. Aqueous 25 v/o WC, 1.8 d.w.p. Duramax 3007 was printed into 300 micron PE spray dried WC/Co.

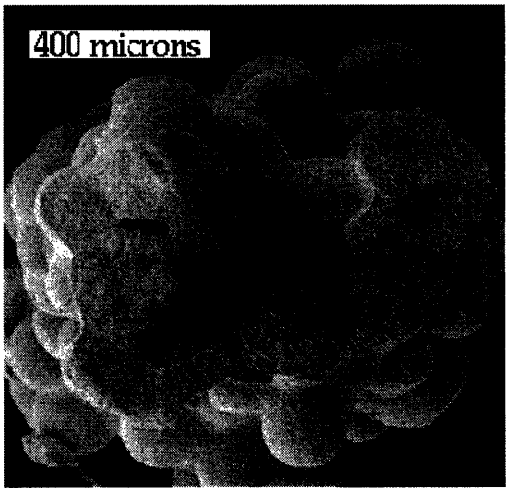

Figure A.3 -- Fractograph of a Line Made by Printing Slurry into PEG Spray Dried WC/Co
The slurry was aqueous 25 v/o WC as mentioned above.

A.3 DISCUSSION

Examining slurry infiltration of solid powder obviated the need for intraparticle void concerns. Further, it served as a base line for the further study of the infiltration of solid powder. In summation, the gating issues for a design based on a slurry infiltration approach alone was that, even the upper packing fraction bound, 0.45, was less than the target of 0.52. Note that the bounds of the packing fraction are dependent upon the slurry solids loading. Also, a critical issue was that the slurry did not stay at 100% saturation. Without the combination of some other approach, carbon dioxide gettering for example, this path was not tenable.

APPENDIX B -- SLURRY INFILTRATION OF CELLULOSE

Highly loaded slurries are used directly in a rapid prototyping process that is protected by intellectual property outside 3DP. For this reason, high porosity powder beds of cellulose were considered. Cellulose also has the advantage that its fibers may be burned out during sintering. Preliminary tests of Kleenex brand tissue, which is primarily cellulose, showed that it had a packing fraction of 0.15. The packing fraction of 100 micron long cellulose fiber was similar.

Various slurry concentrations were administered to powder beds of 100 micron cellulose. Figure B.1 is a fractograph of the cellulose infiltrated by aqueous 40 volume percent WC, 1.8 d.w.p. Duramax 3007 slurry.

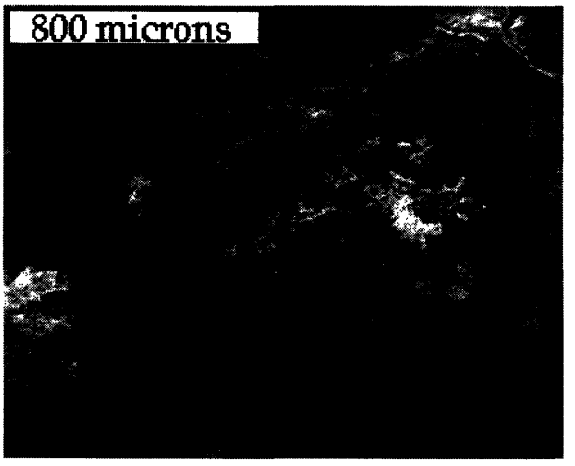

Figure B.1 -- Fractograph of 40 v/o WC into 100 micron cellulose

The primitive packing fractions were so low as to warrant a summary discounting of this approach. The data obtained is tabulated in Table B.1 and shown graphically in Figure B.2. Interestingly, cellulose was the only material system that exhibited an increase in packing fraction with a decrease in solids loading. This phenomenon was attributed to the reduction in rearrangement capacity of the bulky cellulose fibers. Likely, as the slurry dried in the bed, individual fibers disallowed proper rearrangement, especially at high solids loadings.

Solids Loading	Apparent Density (g/cc)	Packing Fraction
0.10	2.11	0.14
0.25	1.58	0.11
0.40	1.45	0.097
0.50	1.28	0.086

Table B.1 -- WC-Cellulose Primitive Data

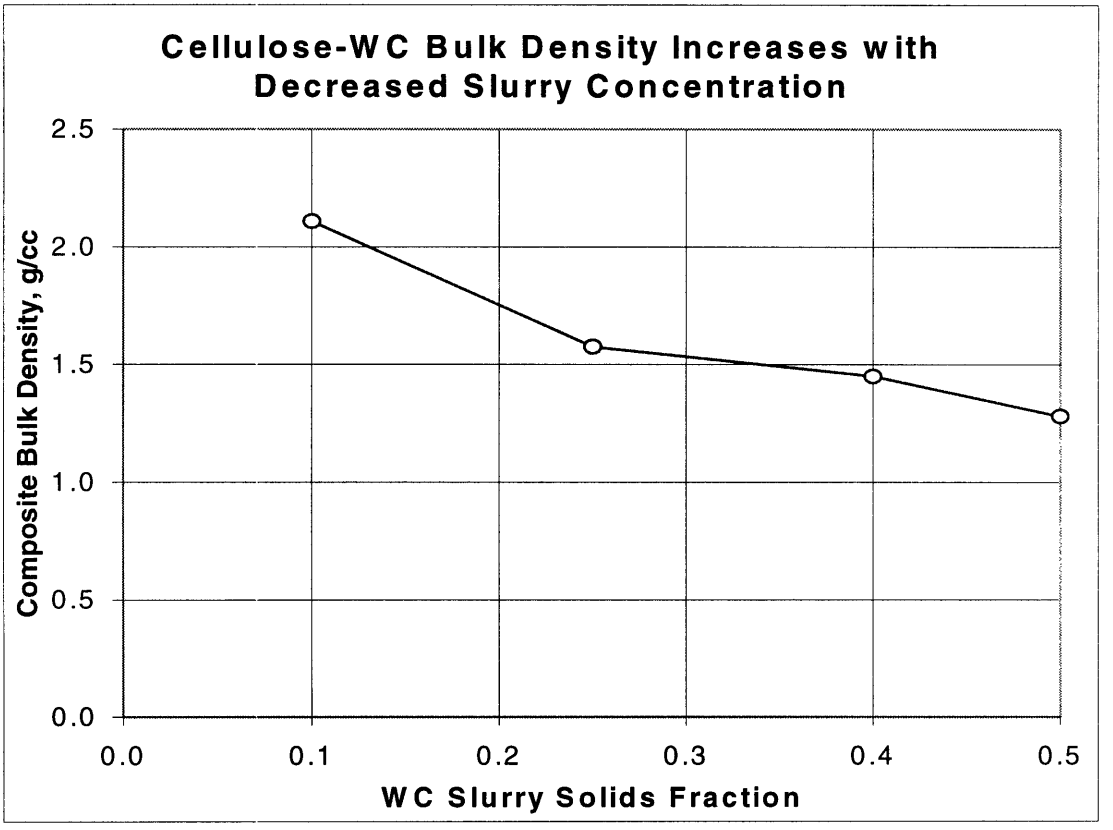

Figure B.2 -- Cellulose-WC Bulk Density Decreases with Solids Loading

APPENDIX C – INFILTRATION SEARCH

Water infiltrated the 0.8 micron WC in less than one second [Caradonna]. However, at room temperature, *twenty minutes* were required for water to infiltrate the 38-53 micron Niro spray dried WC. This was due to Duramax 3007 hydrophobicity. Long infiltration times promote balling and so a search was made for rapid aqueous infiltrants solutions.

Various surfactants and alcohols were added to water. To quickly test many solutions Duramax was dried on a glass slide. A drop of solution was then applied to the slide to assess infiltration potential. The most promising candidates were administered to the 38-53 micron spray dried WC with a syringe.

C.1 CAPILLARY INFILTRATION

Capillary pressure drives infiltration and is governed by the Laplace equation:

$$\Delta P = \sigma_{LV} \cos\theta_{SL}\left(\frac{1}{R_1}+\frac{1}{R_2}\right)$$

where

ΔP	=	infiltration pressure,
σ_{LV}	=	surface tension,
θ_{SL}	=	solid-liquid contact angle, and,
R_i	=	radius of curvature at the liquid vapor interface

For good wetting the contact angle will be small. Initially, the radius of curvature will be on the order of the powder pore radius, R. Under the assumption of a spherical liquid-vapor interface the above reduces to:

$$\Delta P = \frac{2\sigma_{LV}}{R}$$

where $R = R_1 = R_2$.

C.2 SURFACE TENSION AND CONTACT ANGLE

Surface tension is the driving force behind droplet formation in 3DP. The higher the surface tension, the larger the drop of liquid that can be formed at a given pressure. Surface tension for the most rapid infiltrants was measured using Tate's Law [Adamson]. Figure C.1 shows a quasi-free body diagram for a pendant droplet of solution and the corresponding governing equation.

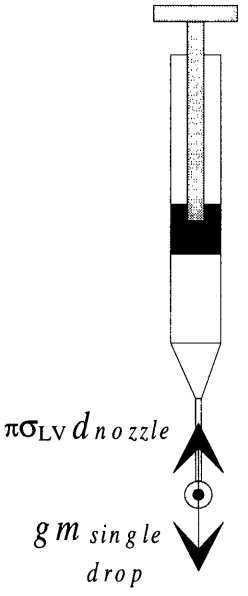

$$\sigma_{LV} = \frac{g m_{\substack{single \\ drop}}}{\pi d_{nozzle}}$$

Figure C.1 -- Tate's Law for Measuring Surface Tension

The syringe was affixed to a 650 micron outer diameter nozzle.

Ten drops of the infiltrant solution were deposited on an analytical balance. The total mass was then divided by ten to determine the mass of a single drop. A 650 micron outer diameter nozzle was used in all surface tension experiments. The outer diameter was used in these calculations since each of the solutions wetted the entire face and periphery of the orifice. Results are shown in Table C.1.

Infiltrant Solution	$t_{infiltration}$ (seconds)	σ_{LV} (N/m)	θ_{SL} (degrees)
30 v/o methanol, H_2O	30	0.042	Negligible
30 v/o IPA, H_2O	90	0.029	Negligible
0.1 w/o Triton X-100, H_2O	480	0.034	Negligible
H_2O	1200	0.0736	< 30°

Table C.1 – Rapid Infiltrant Solution Search Results

The fastest infiltrants contain a large amount of non-aqueous solute. These results confirmed the hydrophobic nature of the spray dried WC. Since Duramax was soluble in water, the contact angle could not be measured directly. Sessile drop measurements of the contact angle were qualitative. A 152 μm nozzle was used to administer the solutions to the WC powder. The droplets were 57 microliters in volume. The powder was 38-53 micron Niro spray dried tungsten carbide.

C.3 PACKING FRACTION

The packing fractions of all of the above single drop primitives were measured. Table C.2 suggests packing fraction decreases with surface tension. For the densest parts the highest surface tension solution, water, should be used. Due to the long infiltration time DOD printing was used to decrease the dosage.

Infiltrant Solution	σ_{LV} (N/m)	ρ_{green} (g/cc)	$f_{packing}$
30 v/o IPA, H_2O	0.029	4.7	0.32
0.1 w/o Triton X-100, H_2O	0.034	5.0	0.34
30 v/o CH_4O, H_2O	0.042	5.0	0.34
H_2O	0.0736	6.2	0.42

Table C.2 – Packing Fraction Decreases with Surface Tension

In each instance, the surface tension was measured at room temperature.
An water displacement (alternative porosimetry) method was used to measure the green density.

APPENDIX D – INK JET SPRAY DRYING

D.1 MATERIALS AND SOLVENT SELECTION

An ink jet spray drier was built to produce highly designed spray dried powder. The design goal was spray dried pellets that dissolved during imbibition. Alumina was chosen as the material system for safety reasons. The powder used was submicron alumina manufactured by Norton. As in conventional spray drying, a number of parameters influence final product.

It was initially desired to produce spray dried alumina pellets of 35 micron diameter. The droplet size for ink jet printing is approximately twice the size of the nozzle orifice. Using a 45 micron nozzle, this corresponded to an aqueous alumina slip loading of 3.8 v/o alumina. Ten volume percent Carbowax 4600 molecular weight polyethylene glycol and 0.05 molar nitric acid were used to disperse the alumina at this loading. Figure D.1 shows an alumina pellet made from this technique. The alumina pellets were on the order of 100 to 200 microns in diameter. However, such a large size could only be accounted for by considering that two or more droplets merged in mid-descent. This morphology was not uniform and was uncharacteristic of most spray dried powder.

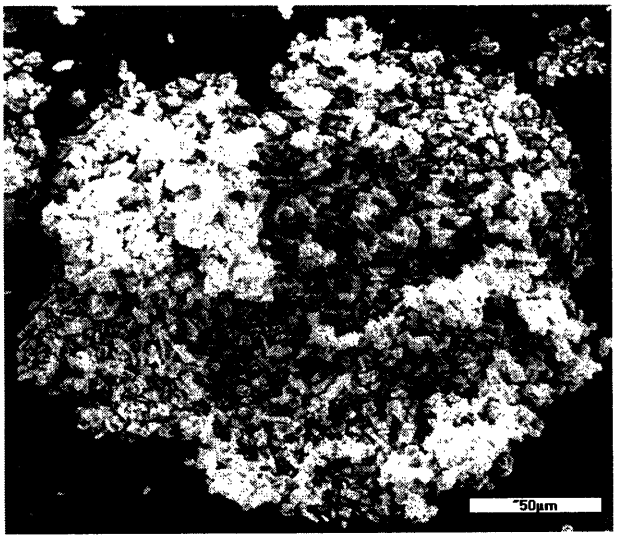

Figure D.1 -- 100 micron Spray Dried Alumina Pellet

D.2 UNIT CONSTRUCTION AND HEATING

Pellets were produced by jetting droplets from a single nozzle in an eight foot high heated enclosure with a two foot square base. The enclosure was made from wood, Kraft paper and, three-eighth inch thick paper-backed urethane foam (foam core poster-board). Clear Plexiglas panels facilitated visualization internal to the unit. Stroboscopic imaging was used to verify that break off occurred within the charging cell. A Leader LFG 1300S function generator supplied the charger voltage, which ranged up to 100 volts. This signal was then amplified by a Krohn-Hite model 7500 amplifier. Spray dried product was collected on a Teflon sheet.

The challenge for this single 45 micron nozzle system was to arrive at the appropriate combination of droplet residence time, jetting parameters, and heat input. Due to space limitations, the unit height could not be substantially increased. Therefore, the residence time of spray dried material in the unit was limited to the free-fall time. A pressure vessel delivered slurry inlet flow rates typically at 1 cc per minute or less. At 1 cc per minute, the production rate was calculated to be 8.9 grams per hour.

Ceramic glow coil heaters were used to provide 1500W of heat internal to the unit. Four heaters were placed in each corner of the unit at elevations of 20, 38, 56 and 74 inches, respectively. The heat input was augmented at times by the introduction of a space heater and or hair dryer. Table D.1 shows a typical internal temperature profile for the spray dryer unit one hour after the heaters were turned on. These temperatures are approximately 100 degrees lower than temperatures typical for conventional spray drying.

Elevation (feet)	Temperature (°C)
1	42
4	99
7	115

Table D.1 -- Manufactured Spray Dryer Internal Temperature Profile after 1 Hour

D.3 DROPLET MERGING

The problem immediately arose that the liquid in the slurry could not be completely dried before the droplets impacted the collection surface. To better understand why drying was incomplete, aqueous 5 v/o standard black or green Hewlett Packard ink was used instead of slurry. By printing onto a white sheet at different elevations, the spray dried plume shape could be determined.

Incomplete drying was evident when residue appeared as a ring and not a solid color dot. Figure D.2 shows the results of incomplete drying due to simple charging. Note the large variation in the wet drop size. The scale in the picture has one-sixty-fourth of an inch markings (615 microns).

Figure D.2 -- Partially Dry Aqueous 5 v/o Ink Droplets
The scale has 1/64" markings.

Figure D.3 shows the difference between simple charging versus charging and deflecting the incoming slurry stream. In the scenario on the left hand side, electrostatic repulsion driven by negatively charged droplets tended to randomly spread the incoming stream. The higher the charger voltage, the greater the charge transferred to the particles and the higher their tendency to repel each other. This higher the electrostatic repulsion, the greater the plume diameter at a given elevation.

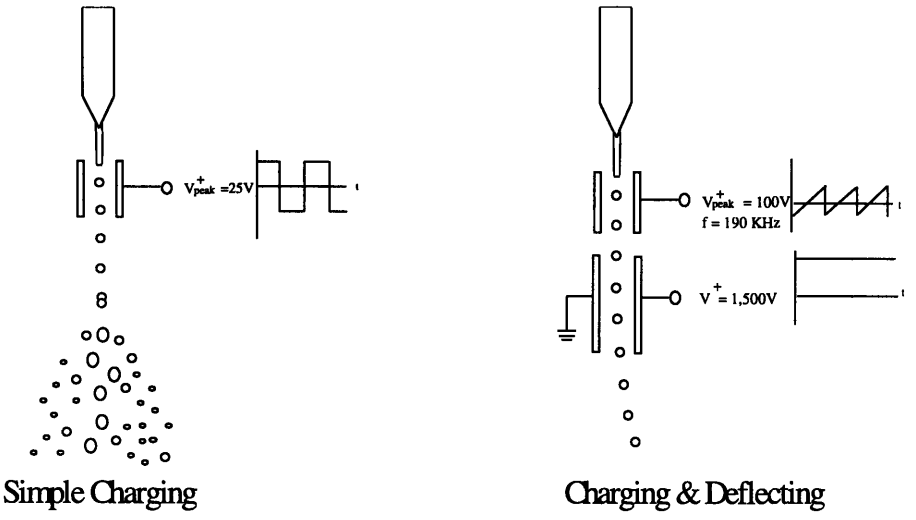

Figure D.3 -- Simple Charging versus Charge and Deflection Spray Drying

The limitation on the charger voltage was such that the droplets were not substantially predisposed to collect on the walls of the unit. A confounding factor was the tendency of the jetted droplets to wander. This was because, having little mass, the convective heating currents tended to move the droplets easily. Also, larger faster drops could have overtaken and merged with droplets that had reached terminal velocity.

To ensure droplet evaporation before impact, 95 v/o methanol, 5 v/o water was jetted with only the glow coils. Figure D.4 below shows the plume diameters at various free stream lengths for this formulation. No heating was input to the unit during this experiment. Droplets were palpable at the floor of the unit for charger voltages greater than 40V. The inflection points between 6 and 18 inches indicated a maximum charge that could be held by the droplets.

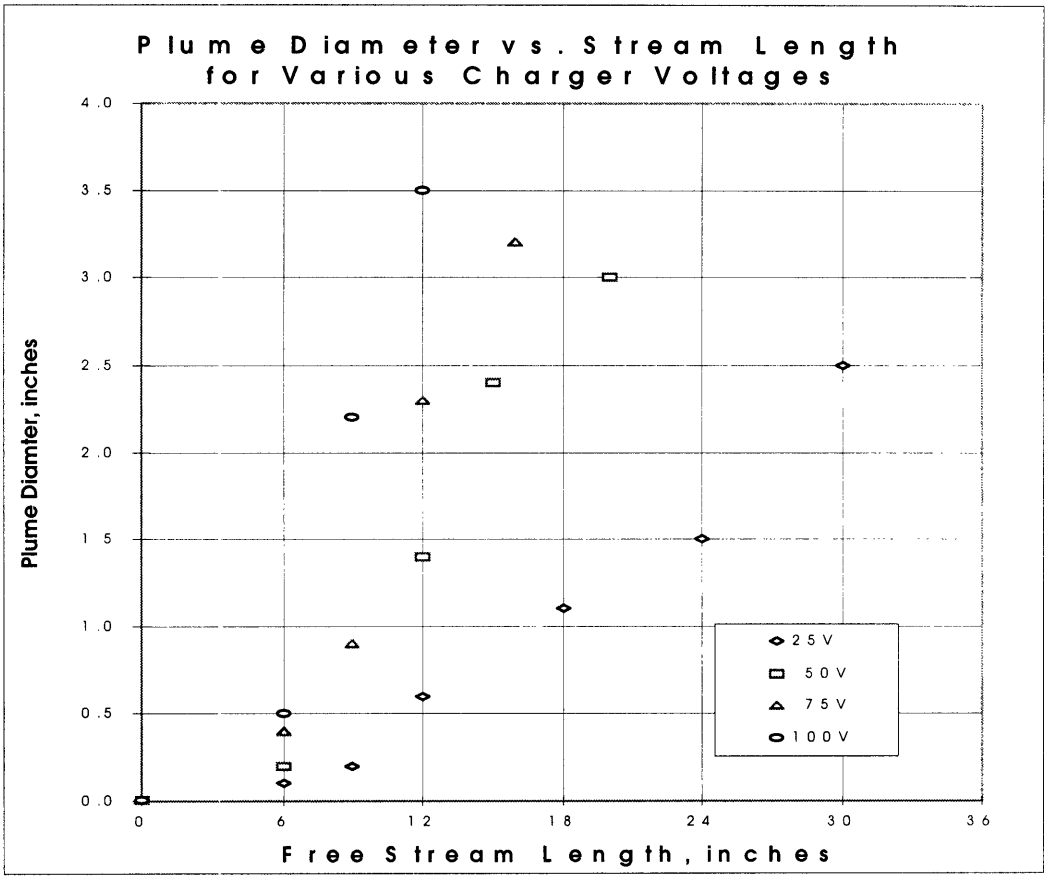

Figure D.4 -- Plume Geometry versus Free Stream Length at Various Charger Voltages

To eliminate merging, each droplet was charged and deflected to a trajectory different than either the preceding or following droplet. This ideas is shown on the right hand side of Figure D.3. The idea was to put enough distance between pellets so that there would be no chance for droplet merging. The deflection voltage was supplied by a Bertan Associates model 205B-03R high voltage DC supply. However, this approach was unsuccessful even with volatile solvents.

Carbowax polyethylene glycol dissolves in neither methanol nor acetone. Therefore, alumina slurries with a methanol-water base would be unstable with PEG as a dispersant. Despite the fact that 95 v/o methanol solution could be dried, more massive spray dried droplets, could not. In the end, the yield and resource limitations of this method detracted from its promise in a material fashion. The termination of work down this path allowed for more exploration down the path of jetting slurry into spray dried powder.

APPENDIX E -- MERCURY AND ALTERNATIVE POROSIMETRY

E.1 MECURY POROSIMETRY EXAMPLE -- CARBON DIOXIDE GETTERED PRIMITIVE

The following examples illuminate the calculations of the shrink-wrapped volume of a primitive as determined using mercury porosimetry. The primitives in this case were made by quenching the powder bed from 23 °C to o°C in seven minutes. That is, these were the pellets made by gettering carbon dioxide with water. The porosimetry plot is given again in Figure E.1 for ease of reference.

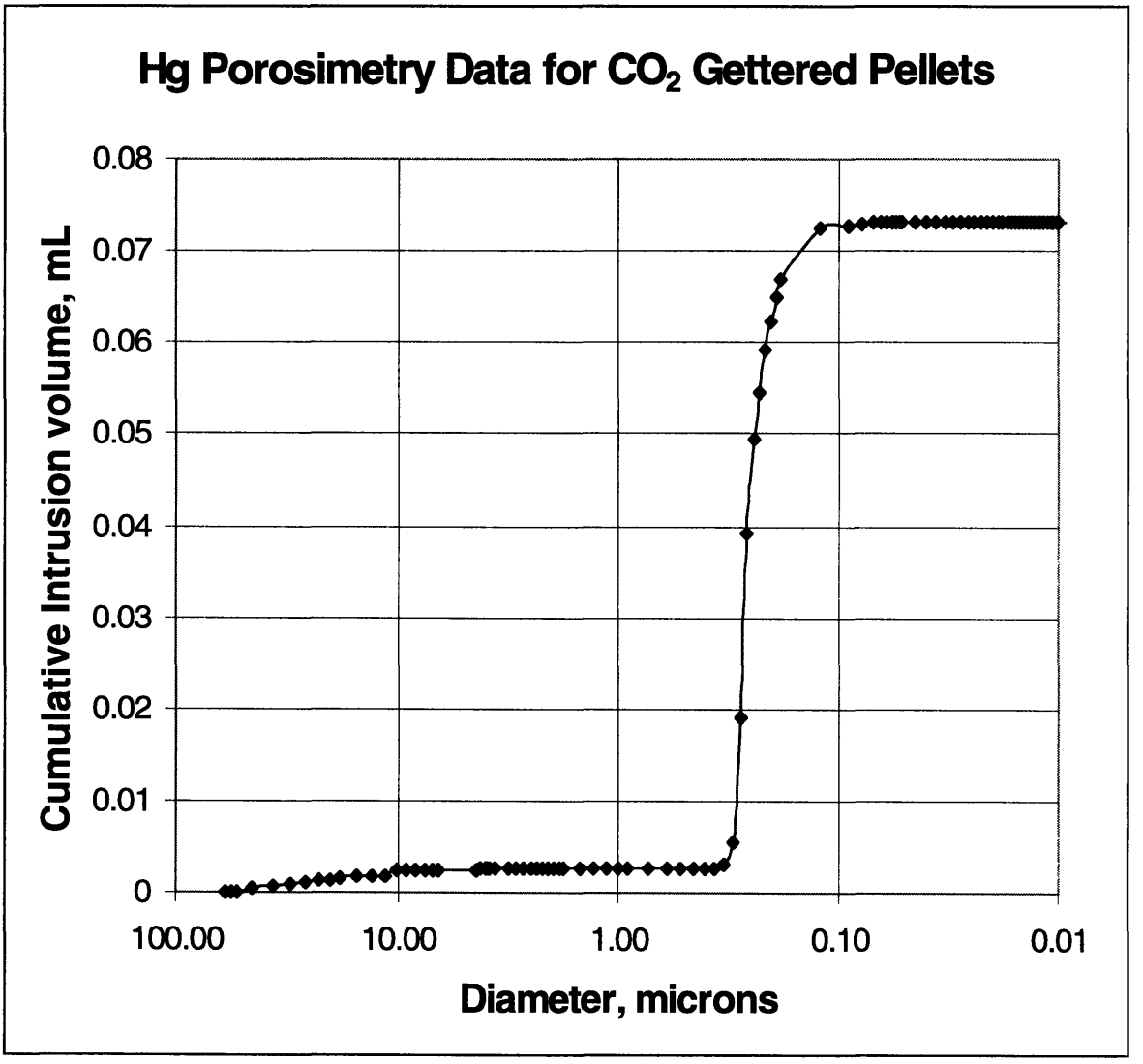

Figure E.1 -- Porosimetry Data for Carbon Dioxide Gettered 38-53 micron Spray Dried WC

The shrink-wrapped volume, v_{sw}, of a primitive was defined as the volume that uniformly encapsulates the outer surface of that primitive in its entirety. The shrink-wrapped volume of a sample could be calculated from mercury porosimetry data and was useful for calculating the green density. The green density was determined by dividing the sample mass by the shrink-wrapped volume.

A clean and calibrated penetrometer was used for each mercury porosimetry run. The bulb volume of the penetrometer was known very precisely, typically to 0.0001 cc. Each penetrometer bulb had been calibrated with a matching cap. The bulb volume for the sample in this illustration was 3.2039 cc.

Approximately 30 pellets used during this run. The mass of the primitives added to the bulb was 1.341 grams. These pellets were placed inside of the bulb which was then greased and capped. The entire assembly was then weighed on an analytical balance. The mass, labeled m_1 below, was noted. The assembly was then placed in one of the four low pressure ports in the mercury porosimeter.

The low pressure run was then initiated through the Micromeritics software. Each low pressure run took approximately three hours to complete and ended at a pressure of approximately 30 psia. The pressure measured internal to the system was used to calculate the corresponding pore diameter using the Laplace equation. This pressure always corresponded to a pore diameter of 7 microns.

After the low pressure run was complete, the assembly was removed from the machine. The assembly mass was measured using an analytical balance. This mass, labeled m_2 below, was 111.001g. At this point, the assembly consisted of the penetrometer, the sample and the mercury which had infiltrated the penetrometer bulb at low pressure. The volume of mercury that filled the bulb and stem was labeled v_{Hg} below.

The temperature of the mercury porosimeter was noted at the end of the low pressure infiltration run. The density of mercury at that temperature, 28°C, was 13.5266g/cc.

Finally, the amount of mercury that infiltrated any large porosity was taken into account. This over-infiltration of the sample by mercury was accounted for in each case and required that the addition of a small correction volume, v_{cor}, to the sample volume. The correction volume was the elevation of the mercury porosimetry curve corresponding to the transition from the low pressure to the high pressure run, 7 microns. For very porous samples, such as loose spray dried powder, this correction is significant. For this case, where the sample was very much like a slip casting, the term was not.

For the purpose of determining the shrink wrapped volume of the sample, it is not necessary to complete a high pressure mercury porosimetry run for very dense samples. This high pressure run would range from 30 psia to 60 psia. The transition from low pressure run to the high pressure run always occurred at 30 psia. Since, the pore diameter was determined in the software by using the Laplace equation, this always corresponded to a transition point of 7 microns. The chief reason to perform a high pressure run is the resulting sample pore structure information which is not easily obtainable otherwise. One of two high pressure ports could have been used for this purpose. Experience will guide the need for added effort. To summarize the variables, let:

v_{sw} = the shrink-wrapped sample volume,
v_{pen} = the volume of the penetrometer bulb and stem,
m_1 = the mass of the penetrometer and sample before Hg infiltration,
m_2 = the mass of the penetrometer and sample after Hg infiltration at low pressure,
v_{Hg} = the volume of mercury that infiltrated the penetrometer at low pressure,
ρ_{Hg} = the density of mercury at the infiltration temperature, and,
ρ_{bulk} = the apparent or bulk density of the primitives measured
v_{cor} = the volume of mercury which must be subtracted from the reported volume to correct for over-infiltration of the sample.

After all of the above data was collected, the shrink-wrapped volume of the sample could then be calculated:

$$v_{sw} = v_{pen} - v_{Hg} + v_{cor}$$

Note that the mass of the mercury which infiltrated the sample would be

$$\text{mass of mercury} = m_2 - m_1$$

Therefore,

$$v_{sw} = v_{pen} - \frac{m_2 - m_1}{\rho_{Hg}} + v_{cor}$$

And substitution yielded

$$v_{sw} = 3.2039\text{cc} - \frac{111.001g - 70.130g}{13.5266g/cc} + 0.0024\text{cc}$$

$$v_{sw} = 0.1848\text{cc}.$$

Therefore, the bulk density was

$$\rho_{bulk} = \frac{1.341g}{0.1848cc}$$

$$\rho_{bulk} = 7.26\ \text{g/cc}$$

And the packing fraction for this run was,

$$f_{packing} = \frac{7.26g/cc}{14.9g/cc}$$

$$f_{packing} = 0.487.$$

E.2 MERCURY POROSIMETRY EXAMPLE -- 38-53 MICRON SPRAY DRIED WC

As an additional example, the same procedure will be outlined for 38-53 micron Niro spray dried powder. The porosimetry plot is given again in Figure E.2 here for ease of reference.

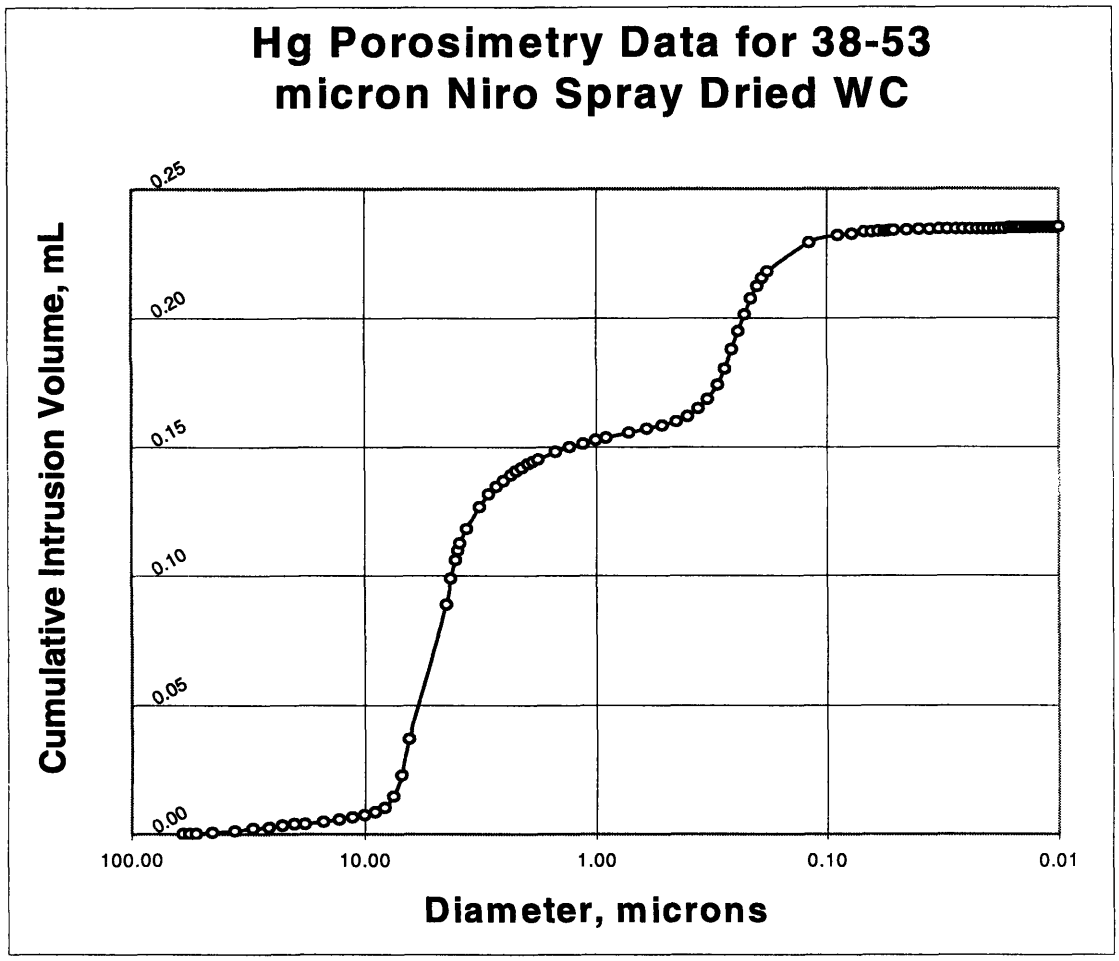

Figure E.2 -- Porosimetry Data for the 38-53 micron Niro Spray Dried WC

The most significant difference between this sample and the previous was the number of large voids greater than 1 micron. These were nearly absent in the previous sample. The transition from the low pressure to the high pressure run in mercury porosimeter occurred at 30 psi, or about 7 microns. A high pressure run will always be required to characterize sample porosity for samples with pore distributions below 7 microns.

The bulb volume for the sample in this illustration was also 3.2039 cc. The mass of the spray dried WC powder added to the bulb was 1.4023 grams. These pellets were placed inside of the bulb which was then greased and capped. The entire assembly was then weighed on an analytical balance. The mass, labeled m_1 below, was noted to be 69.4043g. The assembly was then placed in one of the four low pressure ports in the mercury porosimeter.

After the low pressure run was completed, the assembly was removed from the machine. The assembly was weighed and this mass, labeled m_2 below, was 107.8508g. At this point, the assembly consisted of the penetrometer, the sample and the mercury which had infiltrated the penetrometer bulb at low pressure. The volume of mercury that filled the bulb and stem was labeled v_{Hg} below.

The temperature of the mercury porosimeter was noted at the end of the low pressure infiltration run. The density of mercury at that temperature, 29°C, was 13.5242g/cc.

To better characterize the pore structure, it was necessary to complete a high pressure mercury porosimetry run. This was because there was significant porosity below 7 microns in this particular sample. This porosity had a local mean distribution of approximately 5 microns. Refer to Figure E.2. These pores could have been of two different types:

1. pores between the spray dried pellets, or,
2. large porosity within the spray dried pellets.

Recall that many of the spray dried WC pellets were hollow and/or dimpled. Mercury porosimetry could not distinguish between the pores between the spray dried pellets and the pores within the spray dried pellets. Therefore, the shrink-wrapped volume would be overestimated if the volume where to have been increased by an amount equivalent to the volume of the entire first plateau volume, 0.15 cc in all. Had this entire volume been used for the correction, the resulting shrink-wrapped volume, v_{SW}, would have been

approximately 0.52. In turn, the bulk density and packing fraction would have been 2.7g/cc and 0.18. These numbers were, quite clearly, far from the mark. Instead, and more properly, the correction volume, v_{cor}, was taken to be the value of the cumulative mercury infiltration at 7 microns, 0.0037cc.

As before,

$$v_{sw} = v_{pen} - v_{Hg} + v_{cor}$$

$$v_{sw} = v_{pen} - \frac{m_2 - m_1}{\rho_{Hg}} + v_{cor}$$

And substitution yielded

$$v_{sw} = 3.2039\text{cc} - \frac{107.8508g - 69.4043g}{13.5242g/cc} + 0.0037\text{cc}$$

$$v_{sw} = 0.3981\text{cc}.$$

Therefore, the bulk density was

$$\rho_{bulk} = \frac{1.4023g}{0.3981cc}$$

$$\rho_{bulk} = 3.52\ \text{g/cc}$$

Hence,

$$f_{packing} = \frac{3.52g/cc}{14.9g/cc}$$

$$f_{packing} = 0.24.$$

This compares favorable with the value obtained by weighing 10cc of powder in a graduated cylinder. For that experiment, the packing fraction was 0.25.

E.3 ALTERNATIVE POROSIMETRY METHOD

The most important value that must be determined for primitives that were made was the packing fraction. In order to determine this, the shrink wrapped volume of the primitive was required. Since mercury porosimetry was a time consuming process an alternative method was used at times.

In this method, the mass of several primitives was measured using an analytical balance. These primitives were then coated and infiltrated with paraffin wax so that the infiltrating liquid would not penetrate the internal porosity. Excess wax was removed from the primitives by heating them on filter paper.

A volume of liquid was introduced to a cylinder just large enough to accommodate the primitives. The internal diameter of the cylinder was approximately 4 millimeters. The initial liquid volume was then marked on the cylinder. Twelve to 18 single wax coated primitives were added to the cylinder. The apparatus was then placed on an analytical balance which was then tared.

The primitives displaced liquid so that the total height of the column was indicated by the final liquid level as shown in Figure E.1. Liquid was then removed so that the initial liquid level was obtained. This mass of liquid was then divided by the density of the liquid in order to obtain the liquid volume displace, and, hence, the total shrink wrapped volume of the primitives.

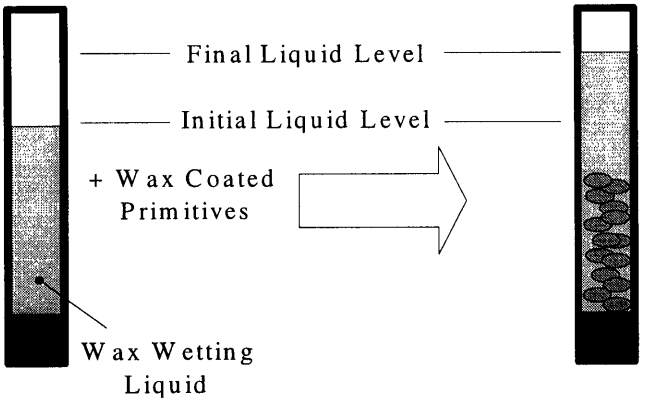

Figure E.3 -- Alternative Porosimetry Apparatus

A comparison of various samples is given in Table E.1 below. The table compares the packing fraction values obtained using this method and those obtained using mercury porosimetry. In each of the cases, two or more samples were run and the average values appear in Table E.1. The relative percentage difference is also given.

Sample	Hg Porosimetry Packing Fraction	Alternative Porosimetry Packing Fraction	Percentage Difference, %
38-53 micron Niro Spray Dried WC Primitives without gettering[1]	0.468	0.447	4.6
38-53 micron Niro Spray Dried WC Primitives with gettering[2]	0.502	0.456	9.6

Table E.1 -- Mercury Porosimetry and Alternative Porosimetry Method Comparison

Primitives were made by administering single drops of water through a 152 micron nozzle.
[1]The wetting liquid used was water.
[2]The wetting liquid used was Multitherm 503.

Note that for the carbon dioxide gettered primitives, Multitherm 503 was used because it wetted wax than water did. This eliminated air bubbles which might have been entrapped in the cylinder once pellets were inserted.

The packing fraction is based on division by the density thus obtained by 14.9 g/cc, the true density of the tungsten carbide. The general trend was that the data obtained using the alternative porosimetry method underestimated the packing fraction. However, the method does provide a relatively painless way to quickly calculate the packing fraction of a number of small primitives.